Trends in Analytical Chemistry 157 (2022) 116806

Contents lists available at ScienceDirect

Trends in Analytical Chemistry

journal homepage: www.elsevier.com/locate/trac

Microfluidic platforms integrated with nano-sensors for point-of-care bioanalysis

Hamed Tavakoli [a], Samayeh Mohammadi [a], Xiaochun Li [b], Guanglei Fu [c, **], XiuJun Li [a, d, *]

[a] Department of Chemistry and Biochemistry, University of Texas at El Paso, El Paso, TX, 79968, USA
[b] College of Biomedical Engineering, Taiyuan University of Technology, Shanxi, 030606, China
[c] School of Pharmacy, Key Laboratory of Molecular Pharmacology and Drug Evaluation, Ministry of Education, Collaborative Innovation Center of Advanced Drug Delivery System and Biotech Drugs in Universities of Shandong, Yantai University, Yantai, Shandong, 264005, China
[d] Border Biomedical Research Center, Forensic Science, & Environmental Science and Engineering, University of Texas at El Paso, El Paso, 79968, USA

ARTICLE INFO

Article history:
Received 13 September 2022
Received in revised form
24 October 2022
Accepted 24 October 2022
Available online 29 October 2022

Keywords:
Bioanalysis
Point-of-care detection
Microfluidic platforms
Nano-sensors
Nanotechnology

ABSTRACT

Microfluidic technology provides a portable, cost-effective, and versatile tool for point-of-care (POC) bioanalysis because of its associated advantages such as fast analysis, low volumes of reagent consumption, and high portability. Along with microfluidics, the application of nanomaterials in biosensing has attracted lots of attention due to their unique physical and chemical properties for enhanced signal modulation such as signal amplification and signal transduction for POC bioanalysis. Hence, an enormous number of microfluidic devices integrated with nano-sensors have been developed for POC bioanalysis targeting low-resource settings. Herein, we review recent advances in POC bioanalysis on nano-sensor-based microfluidic platforms. We first briefly summarized the different types of cost-effective microfluidic platforms, followed by a concise introduction to nanomaterial-based biosensors. Then, we highlighted the application of microfluidic platforms integrated with nano-sensors for POC bioanalysis. Finally, we discussed the current limitations and perspective trends of the nano-sensor-based microfluidic platforms for POC bioanalysis.

© 2022 Elsevier B.V. All rights reserved.

1. Introduction

Bioanalysis technologies have improved significantly over the past few decades [1,2]. Automation of laboratory bioanalysis tests enhances reliability and reduces operator time in developed countries. But most advanced bioanalysis technologies need highly trained staff and specialized facilities. In addition, the required equipment is usually costly and bulky [3]. Therefore, many laboratory-based bioanalysis tests regarded as standard in developed countries are cost-prohibitive and inaccessible to clinicians in many other countries [4]. The World Health Organization (WHO) and others have called for new bioanalysis methods that can function in settings with limited access to an equipped laboratory. Point-of-care (POC) bioanalysis is a type of tests that can be completed at or near the care site or other low-resource settings, and provide instant results without waiting days or even hours for sample transport and laboratory processing [5,6]. The POC bioanalysis began in 1962 by developing a rapid blood glucose concentrations measurement method [7]. POC technology shifted bioanalysis from conventional diagnostic assays in clinical laboratory settings to near-patient settings, providing timely diagnostic and treatment information. POC bioanalysis presents numerous advantages such as ease of operation, low cost, the ability to provide rapid and accurate results, and little need for specialized instruments [8–11]. The emergence of POC bioanalysis can improve healthcare services and patient-centered outcomes in diverse settings, especially low-resource settings.

Microfluidic lab-on-a-chip (LOC) platforms have been developed quickly in the last two decades [12–14], presenting versatile applications in chemical, biomedical, biological, and environmental fields [15–21]. Microfluidic devices are miniaturized and only need a small volume of body fluid, making them highly suitable for bioanalysis such as diagnosis of infectious diseases and cancer [22–29]. LOC technology has several advantages for POC bioanalysis assays, such as small reagent consumption, cost-efficiency, integration, portability, and less need for experienced personnel to

* Corresponding author. Department of Chemistry and Biochemistry, University of Texas at El Paso, El Paso, TX, 79968, USA.
** Corresponding author.
E-mail addresses: fuguanglei@ytu.edu.cn (G. Fu), xli4@utep.edu (X. Li).

https://doi.org/10.1016/j.trac.2022.116806
0165-9936/© 2022 Elsevier B.V. All rights reserved.

operate [30]. That's why the microfluidic biochips have attracted increasing interest in both scientific research and practical applications by providing inexpensive platforms for POC applications. However, it is still challenging for cost-effective microfluidic devices to achieve high-sensitivity POC bioanalysis with minimal instrumentation.

Nanomaterials have excellent potential in biosensing systems because of their unique chemical and physical characteristics [17,31,32]. Materials in the nanoscale size range have unique structural and functional properties that are not available from bulk materials or small molecules, which make them ideal probes for many applications [33–36]. Nanomaterials offer outstanding optical, photophysical, electronic, and catalytic properties [37–40]. Generally, the optical (e.g., colorimetric, fluorescent, and surface plasmon resonance (SPR)) and electrochemical properties of nanomaterials are most extensively applied in developing biosensors [41,42]. For example, nanoparticles (NPs) with eminent extinction coefficients at desirable wavelengths, visible color changes upon varying dimensions or dispersity, and fluorescence emission are ideal candidates for constructing optical biosensors, such as colorimetric and fluorescent ones [42,43]. Some other NPs with good electronic conductivities or electrocatalytic activities are good choices for electrochemical biosensors [26,44]. It is worth noting that, in some cases, multiple nanomaterials work together in a single biosensor while contributing these properties. Furthermore, metallic nanoparticles confine their electrons and produce quantum effects and a higher quantum yield for biosensing due to the extremely small size [45]. Dye-doped and semiconductor crystal nanoparticles present good fluorescent properties [46]. Functionalization and modification of nanomaterials with biomolecules such as antibodies, enzymes or oligonucleotides can effectively improve the analytical performance in bioanalysis [47,48]. All these properties make nanoparticles ideal candidates for developing novel signal generation and amplification strategies for bioanalysis [49–54] which can complement microfluidic devices for POC biosensing, especially in signal amplification and transduction such as colorimetric detection readout from gold nanoparticles (AuNPs) [27]. Their combination brings tremendous advantages and potential for rapid, low-cost, and high-sensitivity POC analysis for low-resource settings. Therefore, the integration of nanomaterials on microfluidic devices for point-of-care bioanalysis has attracted considerable attention due to the demands for ultrasensitive and high-throughput bioanalysis [17,23,55,56].

This article reviews the most recent advances in microfluidic technologies integrated with nanomaterials for bioanalysis. We first briefly introduce different cost-effective microfluidic platforms for bioanalysis. Then, we summarize different types of nanoparticles commonly applied in biosensing, followed by various applications of microfluidics integrated with nano-sensors for POC bioanalysis. Finally, we discuss the current limitations of nanosensor-based microfluidic POC bioanalysis and perspectives.

2. Cost-effective microfluidic devices

Since the advent of microfluidic lab-on-a-chip in the 1990s [14], a diverse range of materials have been used to fabricate various types of microfluidic LOC platforms for different applications [57–59]. Silicon, glass, polymeric substrates, cellulosic substrates, and some emerging biomaterials are the most applied materials in the fabrication of microfluidic devices [28,60–63]. Polymer substrates and paper recently attracted lots of attention for fabricating cost-effective microfluidic devices [30,55]. Based on the materials of substrates used in microfluidic device fabrication, microfluidic LOC platforms can be categorized as single-substrate and hybrid microfluidic platforms. The cost-effective single-substrate microfluidic platforms are mostly fabricated using polymer substrates (e.g., Polydimethylsiloxane (PDMS) and Poly (methyl methacrylate) (PMMA)) and paper substrates [64–66]. Polymer/paper hybrid microfluidic devices can draw more benefits from different chip substrates, and thus have drawn more and more attention in microfluidic and bioanalysis fields and offered cost-effective, versatile platforms for nucleic acid analysis, protein detection, cellular analysis, etc [25,67,68]. This section briefly summarizes polymer-based, paper-based, and paper/polymer hybrid cost-effective microfluidic devices.

2.1. Polymer-based microfluidic devices

Reduced production costs, flexibility, ease of fabrication, rapid prototyping, and no need for hazardous etching reagents make polymeric materials more popular than glass in fabricating cost-effective microfluidic devices. Thermoplastics (e.g., PMMA) and elastomers (e.g., PDMS) are two main polymeric substrates applied to fabricate microfluidic devices. PMMA has good compatibility with the mass production techniques [69]. Several fabrication techniques such as laser ablation, injection molding, and micro-milling were applied to make microfluidic platforms using PMMA [30,70]. PMMA-based microfluidic devices can withstand high pressure because PMMA is rigid below the glass-transition temperature. Moreover, PMMA presents several advantages such as low intrinsic fluorescence, broadly visible transmittance, good chemical stability, and biocompatibility. Several PMMA-based microfluidic devices were presented for bioanalysis [71,72]. For example, Kim et al. developed a PMMA-based microfluidic platform by bonding two PMMA plates through acetone injection using a customized press machine [71]. The device was used for POC detection of H1N1 Influenza A. The linear dynamic range between 0.1 and 1 ng/ml and the limit of detection (LOD) of 0.1 ng/ml were achieved. Yang and coworkers fabricated a microfluidic device in optically transparent PMMA to evaluate the electro-taxis of different lung cancer cell lines [72]. The device presented well-controlled and stable direct current electric field (2–6 V/cm), in which lung cancer cell electrotactic responses including cell migration, directedness, and morphology change were analyzed under a series of electric stimuli. The nonspecific surface adsorption of sample molecules on PMMA and its gas impermeability are some drawbacks of PMMA.

PDMS is the most common material used in microfluidic platform fabrication. PDMS can replace glass at a reduced cost in most optical applications because of its optical transparency. In addition, the permeability of PDMS to gas makes PDMS-based microfluidic platforms appropriate for cellular analysis and long-time cell culture. PDMS was broadly used to fabricate microfluidic devices for POC bioanalysis. For instance, Yin et al. applied multi-layer soft lithography technology to fabricate a PDMS-based microfluidic device [73]. The device was integrated with multiplex digital recombinase polymerase amplification (ImdRPA) to combine DNA extraction, multiplex digital RPA and fluorescence detection together on a single chip. The LOD of the ImdRPA microfluidic platform was 10 bacterial cells. Hao et al. fabricated a PDMS-based microfluidic biochip using a standard soft lithography procedure to detect E. *coli* O157:H7 [74]. Generations of 7-polyamidoamine dendrimers were immobilized onto the detection surfaces of PDMS microfluidic channels; subsequently, aptamers against E. *coli* O157:H7 were conjugated onto the microchannel surfaces via the immobilized dendrimers as templates. The microfluidic platform detected E. *coli* O157:H7 as low as 100 cells/mL. One of the main disadvantages of PDMS-based microfluidic devices is the low specificity and sensitivity of on-chip assays because of nonspecific adsorption of biomolecules. Moreover, exposure to reactive

chemicals can cause the degradation of PDMS [4,75].

2.2. Paper-based microfluidic devices

In the last decade, paper has emerged as a low-cost substrate for fabricating microfluidic platforms [18]. The main advantages of paper substrates are extremely low cost, wide availability, disposability, user-friendliness, ease of fabrication, and compatibility with large-scale manufacturing [76,77]. Inkjet printing, wax printing, and photolithography are usually used to fabricate microfluidic paper-based analytical devices (μPADs) [30]. Integration of various functionalized components on the μPADs makes them good candidates for developing POC bioanalysis systems. Capillary forces control sample handling through the patterned hydrophobic barriers on the μPADs without requiring pumps. Ruecha et al. used a wax-printing technique to fabricate a paper-based microfluidic device coupled with a label-free electrochemical impedance immunosensor for detection of human IFN-γ [78]. A linear relationship between impedance and logarithmic concentrations of human IFN-γ was found in a range of 5–1000 pg/mL with a LOD of 3.4 pg/mL. In addition, Fan et al. developed a paper-based electrochemical immunosensor for the detection of cancer antigen 125 (CA125) by screen-printing technique [79]. The reduced graphene oxide/thionine/gold nanoparticles nanocomposites were coated onto the working electrode of the immunosensor for CA125 antibody immobilization and detection signal amplification. A linear range of 0.1–200 U/mL and the LOD of 0.01 U/mL were achieved. μPADs still face challenges such as significant variations in specificity and sensitivity, the weak mechanical property, low resolutions of patterned microstructures, lack of optical transparency, and low performance in liquid control [80].

In addition to the large-scale fabrication methods, some other techniques such as pen writing-based, and knife cutting-based methods were also presented for fabricating paper-based microfluidic devices [81]. For example, Liu et al. developed a "Pen-Writing" method for providing hydrophobic barrier-free patterned biosensor fabrication and user-friendly bioassay operation [82]. A rollerball pen with reagent ink was applied to directly write on-demand patterned paper biosensors of any design. The single-step glucose biosensor and multi-step immunosensor were prepared, and the multi-analyte detection capability was presented. To perform continuous, high-throughput fabrication and analysis, an automatic platform via combining the reagent ink-based rollerball pen and a desktop pen plotter was also proposed.

2.3. Paper/polymer hybrid microfluidic devices

Hybrid microfluidic devices can present combined merits of different substrates while avoiding the drawbacks of individual substrates. The limitations of the different single-substrate microfluidic platforms have engaged the development of hybrid microfluidic devices, especially cost-effective polymer/paper hybrid microfluidic platforms [30,55]. The first paper/PDMS hybrid biochip was developed by the Li group for pathogen detection [55]. The platform included a top PDMS layer for reagent delivery with inlet reservoirs and one shared waste reservoir, a bottom PDMS layer with 96 microwells for incubation and detection, a piece of chromatography paper placed inside each microwell, and a glass slide as the support. As shown in Fig. 1A, aptamer-functionalized graphene oxide (GO) nano-biosensors were integrated into the chip for simple, one-step, multiplexed pathogen detection. The porous paper inside detection wells in the paper/PDMS hybrid microfluidic platform provided a simple three-dimensional (3D) substrate for nano-sensor immobilization and facilitated the physical absorption of aptamer nano-biosensors without complicated surface modification, a benefit of this paper/polymer hybrid microfluidic device. *Lactobacillus acidophilus* was used as a bacterium model to develop the microfluidic biochip with the LOD of 11.0 CFU/mL. This hybrid device was successfully applied for the multiplexed detection of two infectious foodborne pathogens, *Staphylococcus aureus* and *Salmonella enterica*, with LODs of 61.0 CFU/mL and 800 CFU/mL, respectively. The one-step 'turn on' pathogen detection took about 10 min to complete using the hybrid microfluidic device. In addition, another paper/PDMS hybrid microfluidic device integrated with loop-mediated isothermal amplification (LAMP) for instrument-free diagnosis of bacterial meningitis was reported [83]. In the hybrid microfluidic platform, a chromatography paper disc was inserted into each of the LAMP zones (Fig. 1B). The paper substrate inside the hybrid microfluidic device facilitated the uniform distribution of primers for LAMP reactions. The hybrid microfluidic biochip offered a stable diagnostic performance for a much longer period than a paper-free non-hybrid device (Fig. 1B and c). The performance of LAMP reactions from hybrid microfluidic biochip with paper inside maintained 94% and 85% after 2 and 3 months, respectively. However, the LAMP performance from non-hybrid microfluidic devices without paper inside was reduced by about 40% after 2 months. More recently, the Li group reported a reusable and cost-effective PMMA/paper hybrid plug-and-play (PnP) device for high-sensitivity immunoassay [25]. The PMMA platform had multiple slots where a pre-patterned paper substrate could be placed. The sample flowed back-and-forth through the 3D paper substrate within the PMMA channels, therefore additional amounts of the analyte were adsorbed, and the sensitivity was enhanced while the assay time was decreased. After the enrichment step, the paper substrate could simply be pulled out of the chip, and the results could be qualitatively observed with the naked eye or scanned through a simple desktop scanner for quantitative analysis. The paper substrate could be replaced with a new paper substrate so that the chip could be reused. The LODs of 200 pg/mL for immunoglobulin G (IgG) and 270 pg/mL for hepatitis B surface antigen (HBsAg) were achieved.

Recently, 3D printed paper/polymer hybrid microfluidic platforms were developed for automated bioassays. For example, Yafia et al. introduced the microfluidic chain reaction (MCR) as the conditional, structurally programmed propagation of capillary flow events [84]. The microfluidic devices were three-dimensionally printed and powered by the free energy of a paper pump, and autonomously executed liquid handling algorithms step-by-step. The devices integrated with MCR were applied for automated bioassays including (I) the sequential release of 300 aliquots across chained, interconnected chips, (II) a protocol for severe acute respiratory syndrome-coronavirus-2 (SARS-CoV-2) antibodies detection in saliva, and (III) a thrombin generation assay by continuous subsampling and analysis of coagulation-activated plasma with parallel operations including timers, iterative cycles of synchronous flow and stop-flow operations. A 3D printer was applied to fabricate the chips using a transparent resin. After printing, the chips were cleaned with isopropanol and post-cured for 1 min under ultraviolet (UV) light. Microchannels with cross-sections were hydrophilized by plasma activation for 10 s at approximately 30% power. Filter papers (Whatman filter paper grade 4, 1 and 50) were used as paper capillary pumps for all experiments except the SARS-CoV-2 antibody assay. For the SARS-CoV-2 antibody assay, absorbent pads (Electrophoresis and Blotting Paper, Grade 238) were used as pumps.

3. Nanomaterial-based biosensors

In the past decades, with the enormous advancement in nanoscience, nanomaterials have shown substantial promise in almost

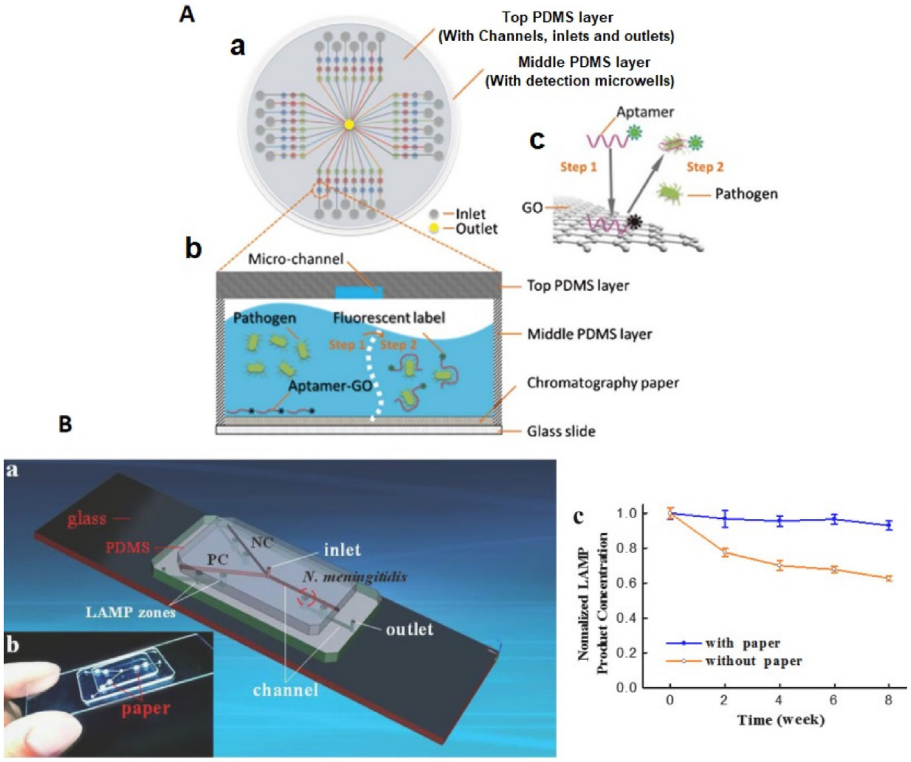

Fig. 1. Paper/polymer hybrid microfluidic platforms for pathogens detection. (A) Schematic of the PDMS/paper hybrid microfluidic device for one-step multiplexed pathogen detection using aptamer-functionalized GO nano-biosensors. (a) Microfluidic biochip layout. (b–c) Illustration of the principle of the one-step 'turn-on' detection approach based on the interaction among GO, aptamers, and pathogens. Adapted with permission from Ref. [55]. Copyright 2013 The Royal Society of Chemistry. (B) The paper/PDMS hybrid microfluidic chip integrated with LAMP for high-sensitivity instrument-free bacterial meningitis diagnosis. (a) 3D illustration of the schematic of the device layout. A chromatography paper disk is placed inside each LAMP zone to preload LAMP primers. (b) A photograph of the hybrid microfluidic platform. (c) On-chip LAMP performance comparison between hybrid microfluidic biochips with paper inside and non-hybrid microfluidic biochips without paper inside. Adapted with permission from Ref. [83]. Copyright 2014 American Chemical Society.

every field, from science to engineering [85,86]. Nanomaterials, defined as tiny materials with external nanoscale dimensions in shapes, possess distinctive physical and chemical characteristics, including large surface area, electrical conductivity, and catalytic activity [41,87]. Nanomaterials are ideal hosts for biomolecule immobilization due to the ease of surface modification. Using these superior properties, nanomaterials have been extensively employed to develop various biosensors utilizing principles such as colorimetry, fluorescence, electrochemistry, and surface plasmon resonance (SPR) [41,88]. As one of the most typical samples, Au nanoparticles (AuNPs) have long served as the immunochromatographic probe in commercial pregnancy test strips.

However, it should be mentioned that the signal readout of some biosensors still has to rely on advanced instruments, such as spectrophotometers [26,89]. The synthesis and modification of some nanomaterials and the analytical procedures are somewhat complex and expensive. In recent years, given the increasing demand for POC testing [22,90], the innovative application of physicochemical properties of nanomaterials has motivated the exploration of new biosensing principles. Numerous promising nanomaterial-involved signal transduction and readout strategies were proposed to develop simple, affordable, and instrument-free bioassays [26,41,87,91,92]. For instance, photothermal effects and catalase-mimic activities of nanomaterials have been exploited as new signal transduction principles to enable visual bioanalysis using portable signal readers, such as thermometers and pressure manometers [91,93]. A lot of work has been focused on the integration of nano-biosensors on microfluidic devices, while playing an integral role in molecule recognition, and signal transduction and modulation (e.g., amplification and quenching). In this section, to lay a basis for the following focus on microfluidic nano-biosensors in the article, we summarily review some representative nanomaterials in biosensors. We then focus on the description of their functional roles in biosensors, particularly for new biosensing principles.

3.1. Types of nanomaterials in biosensing

A vast number of nanomaterials have been synthesized for different applications. In this section, we only focus on those most commonly used nanomaterials for biosensors, namely, gold-based nanomaterials, carbon-based nanomaterials, quantum dots-based nanomaterials, and some other noble metal nanomaterials such as platinum (Pt) NPs. The morphologies of some representative nanomaterials are shown in Fig. 2.

3.1.1. Gold-based nanomaterials

Gold-based nanomaterials can be synthesized in different shapes, including NPs, nanorods, nanoshells, and nanoclusters, among which AuNPs are the most representative [98,99]. Since the first report on using AuNPs for colorimetric assay by Mirkin et al., in 1997 [100], AuNPs have been particularly interested in biosensing applications [101,102]. In addition to the simple synthesis, a broad range of biomolecules and thiol group-terminated grafts can be easily conjugated to the surfaces of AuNPs *via* thiol-Au bonds. Interestingly, upon changing shapes, dispersity, and surface

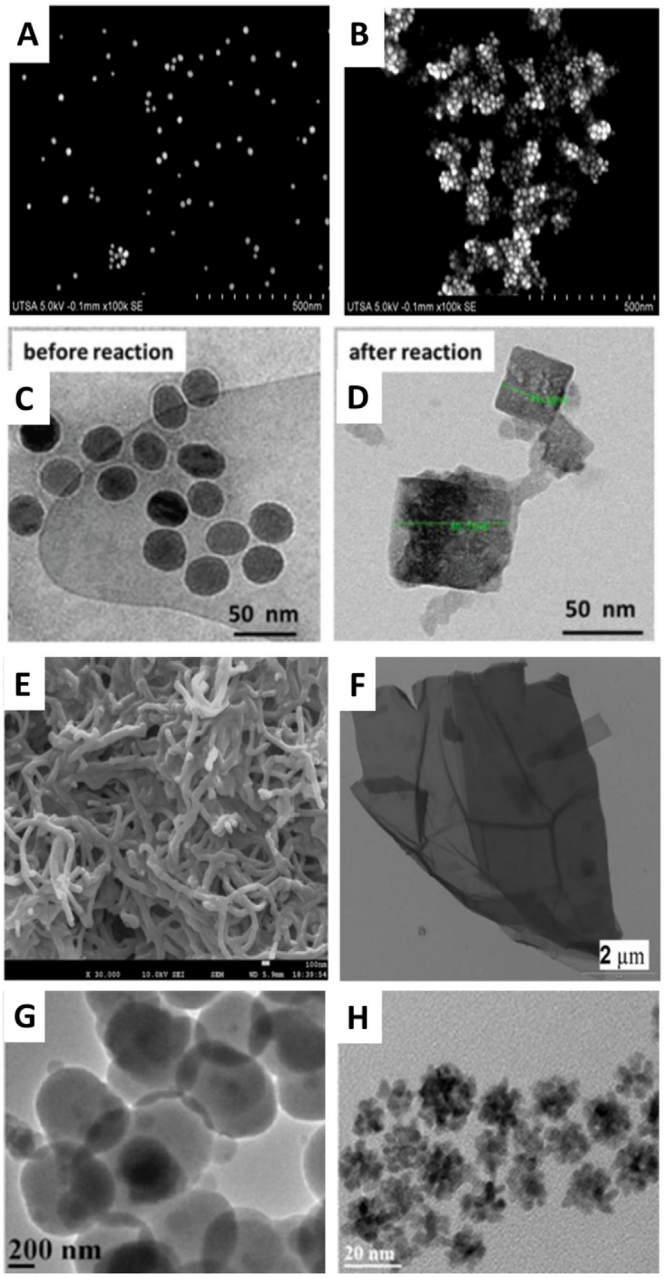

Fig. 2. Morphologies of some representative nanomaterials. (A) SEM images of dispersed gold nanoparticles (AuNPs) and aggregated AuNPS (B) for photothermal biosensing. Adapted with permission from Ref. [27]. Copyright 2021 American Chemical Society. (C–D) TEM images of Prussian blue nanoparticles (PB NPs) (D) transformed from Fe_3O_4 NPs (C) in a photothermal immunoassay. Adapted with permission from Ref. [91]. Copyright 2016 The Royal Society of Chemistry. (E) SEM image of shortened multi-walled carbon nanotubes (S-MWCNTs) in an electrochemical biosensor for microRNAs. Adapted with permission from Ref. [94]. Copyright 2018 Elsevier. (F) TEM image of graphene oxide (GO) nanosheets in a colorimetric bioassay for amphetamine and methamphetamine. Adapted with permission from Ref. [95]. Copyright 2020 Elsevier. (G) TEM image of quantum dots (QDs) in a fluorescent biosensor for chlorothalonil. Adapted with permission from Ref. [96]. Copyright 2020 American Chemical Society. (H) TEM image of platinum (Pt) NPs in a pressure-based biosensor for microRNAs. Adapted with permission from Ref. [97]. Copyright 2021 American Chemical Society.

functionalization, AuNPs show tunable optical properties reflected in forms of external color changes (e.g., from red to blue) and internal changes in the plasmonic behavior (e.g., a shift of plasmonic peaks) [43,98]. In addition, it is demonstrated that AuNPs can dramatically facilitate the electron transfer between immobilized biomolecules and electrode surfaces in electrochemical tests [103]. Hence, AuNPs have been the subject of extensive research for developing colorimetric, electrochemical, and surface plasmon resonance (SPR)-based biosensors [43,104,105].

3.1.2. Carbon-based nanomaterials

To date, the application of carbon-based nanomaterials has become a hot research topic in the biomedical field [106]. With a similar composition of sp^2-hybridized carbon atoms, carbon nanotubes (CNTs) and GO are the most two representative types of carbon-based nanomaterials [42,87]. These carbon nanomaterials, due to their unique nano-composition, retain versatile mechanical and electrical features, such as high surface-to-volume ratio, mechanical flexibility, outstanding electron transportation and inertness to external environments [87,107]. Functional groups like carboxyl groups can be adequately grafted on the edge surfaces of the materials through an oxidation process, making them suitable hosts for biomolecular immobilization and synthesis of other nanomaterials. Furthermore, some ligands and probes (e.g., DNA) can be modified on their surfaces *via* π-π stacking interactions [87]. Therefore, carbon nanomaterials are one of the best choices in developing optical and electrochemical biosensors [108]. In some cases, carbon nanomaterials work with other co-existed NPs as the fluorescence quenchers, modulators of SPR or carriers of colorimetric catalysts [95,109].

3.1.3. Quantum dots-based nanomaterials

As one of the most representative fluorescent probes, quantum dots (QDs), a unique type of semiconductor nanocrystals, have attracted tremendous interest in scientific community [110,111]. The major structure of QDs consists of a core component crystallized by group II-VI or III-V atoms and a shell element mostly comprised of zinc sulfide [87]. Some capping agents are usually utilized to enhance their dispersity in an aqueous medium and for the covalent binding of biomolecules as well [87]. Upon exposure to ultraviolet light, QDs emit vivid fluorescence at wavelengths in the visible light region. The remarkable optical characteristics of QDs include wide absorption bands, high quantum yields, and long fluorescent lifetime, which are of significant advantage for fluorescent imaging and biosensing in comparison with organic fluorophores [112]. The wavelength of emitted fluorescence can be controlled in a broad range by adjusting the size of the nanocrystals interestingly along with the achievement of varying colors of fluorescence [42,87]. In collaboration with other nanomaterials or fluorophores, the fluorescence intensity of QDs can be modulated by molecular-recognition events in biosensors *via* approaches, such as fluorescence resonance energy transfer (FRET) [113,114].

3.1.4. Other nanomaterials

Other noble metal nanomaterials, such as silver (Ag) NPs and platinum (Pt) NPs, have also been widely used in the development of optical and electrochemical biosensors. To some extent, these metal NPs exhibit similar physicochemical functions in biosensing. For instance, like AuNPs, AgNPs and PtNPs possess peroxidase-mimic activities toward some chromogenic substrates, which have been widely used for colorimetric bioanalysis [115,116]. It should be emphasized that PtNPs also have intrinsic catalase-mimic activity [117,118], displaying extensive applications for pressure-based bioanalysis. Recently, some carbon- and metal-based nanomaterials with photothermal effects that can convert light energy into heat energy, such as GO and Prussian blue (PB) NPs, have been applied for photothermal bioanalysis [91,119,120]. Some polymer-based nanomaterials, such as polydopamine NPs, have been also exploited for developing photothermal bioassays

owing to their distinct photothermal effects [121]. In addition, upconversion NPs as a unique kind of luminescent nanomaterials that emit visible lights upon excitation of near-infrared (NIR) lights are of interest for constructing optical biosensors [122].

3.2. Roles of nanomaterials in biosensing

Nanomaterials can participate in not only biomolecule immobilization but also signal modulation in biosensors. Using nanomaterials as hosts or matrices for biomolecule immobilization is a common role of nanomaterials using routine chemical and physical methods, some of which will be described in the following Application section, but are not the focus of this article. As one of the most critical steps in biosensing, nanomaterials participate in the transduction of molecular-recognition events into measurable signals, namely signal transduction [123,124]. To improve the analytical performance (e.g., sensitivity), modulation of the assay signals by nanomaterials such as amplification and quenching is widely implemented in biosensors [110,125]. We herein mainly focus on these essential roles in biosensing signals, particularly for some new principles in POC testing.

3.2.1. Signal transduction

Nanomaterials can participate in the transduction of molecule-recognition events into measurable signals in biosensors. In signal transduction, nanomaterials usually serve as the signaling probes directly or indirectly associated with the molecule-recognition events [123,124]. The optical (e.g., colorimetric, plasmonic, and fluorescent) signal transduction is one of the most conventional mechanisms in biosensors [41,42,126]. Directly, nanomaterials with desirable signaling properties are labeled with biomolecules (e.g., antibodies and DNA) and specifically linked to the molecule-recognition systems. For instance, Du et al. reported a dual-channel immunochromatographic test strip for simultaneous quantification of cypermethrin and 3-phenoxybenzoic acid (3-PBA) [127]. Polymer carbon dots immuno-captured in the system worked as a fluorescent probe. The fluorescence signal was recorded and analyzed on site by employing a portable smartphone-based device, through which cypermethrin and 3-PBA were detected at LODs of 0.35 and 0.04 ng/mL, respectively. Wei and co-workers proposed an immunoassay for colorimetric and fluorescent detection of dicofol [128]. Nanocomposites of Au–Ag nanoclusters and polyethyleneimine (PEI)-modified AuNPs were labeled with the detection antibody and used as a dual-model colorimetric/fluorescent probe.

Indirectly, the signaling behaviors of nanomaterials or relevant probes are triggered or tuned due to the molecule-recognition events, leading to the detection of target biomolecules. Jiang and colleagues presented several impressive biosensors using AuNPs as the plasmonic probes in POC bioanalysis [98,130,131]. For example, they developed a colorimetric immunoassay for human IgG based on enzyme-triggered click chemistry [129], as shown in Fig. 3A. Alkaline phosphatase (ALP) immuno-captured in an ELISA system triggered the Cu(I)-catalyzed cycloaddition between azide and alkyne groups on AuNPs, realizing the NP aggregation-induced colorimetric signal transduction. In recent years, the catalase-mimic activity of PtNPs has exhibited great promise for pressure-based signal transduction. Jin et al. established a pressure biosensor for the detection of microRNAs (miRNAs) on paper chips (Fig. 3B) [97]. PtNPs were tagged with complementary DNAs to construct a sandwich genetic assay system. The captured Pt NPs triggered the dissociation of H_2O_2 to produce oxygen, and the pressure signal in a sealed environment was measured using a portable pressure manometer. Target miRNAs were quantitatively tested in a linear range from 10 pM to 100 nM. Based on a similar

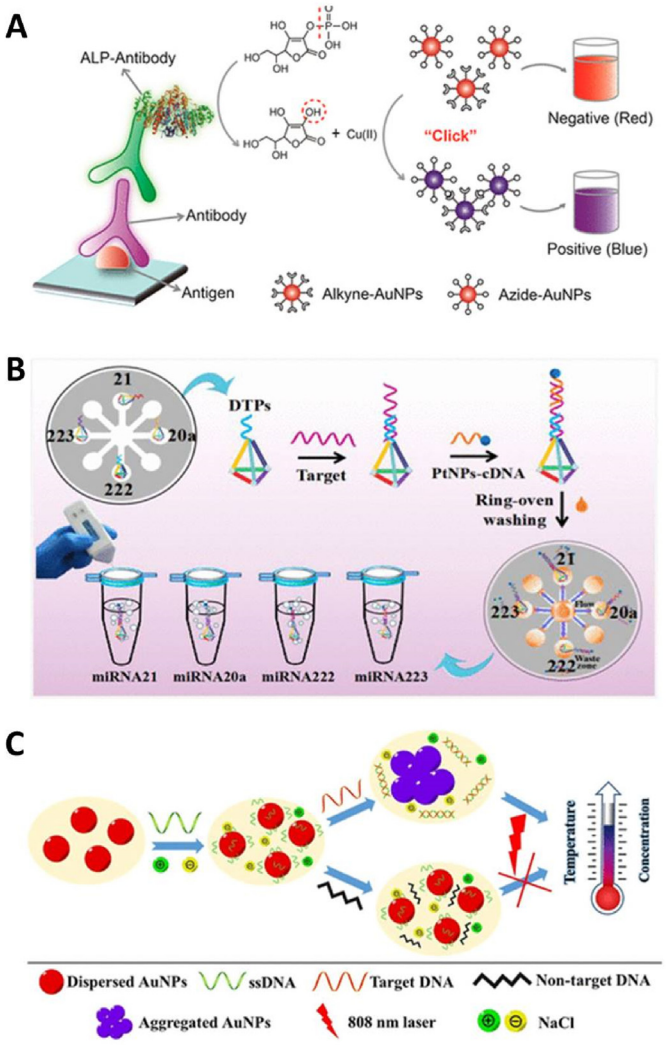

Fig. 3. Schematic illustration of different signal transduction principles of nanosensors. (A) Colorimetric signal transduction in an immunoassay of human IgG using AuNPs as the plasmonic probe. Adapted with permission from Ref. [129]. Copyright 2014 American Chemical Society. (B) Pressure-based signal transduction in detecting microRNAs (miRNAs) using the catalase-mimic activity of PtNPs. Adapted with permission from Ref. [97]. Copyright 2021 American Chemical Society. (C) Photothermal signal transduction in genetic analysis using AuNPs as the photothermal probe. Adapted with permission from Ref. [27]. Copyright 2021 American Chemical Society.

mechanism, Du et al. proposed a POC bioassay for alcohol detection using Pd@Pt core-shell NPs as the probe [132].

Photothermal signal transduction has recently attracted enormous attention for POC bioanalysis because of the ease of visual signal readout using portable temperature readers [91,119,133]. Li's group pioneered this field [24,27,91]. For instance, they innovatively exploited Prussian blue nanoparticles (PB NPs) as a photothermal immunoassay probe for detecting prostate-specific antigen (PSA) [91]. Upon NIR laser irradiation, the photothermal effect converted the immuno-recognition event into heat signals, enabling quantitative immunoassay utilizing a portable digital thermometer as the signal reader. Excitingly, they, for the first time, discovered the NIR light-mediated photothermal effect of the oxidation product ($_{ox}$TMB) of a conventional chromogenic substrate, 3,3',5,5'-tetramethylbenzidine (TMB), and successfully explored it as a new photothermal biosensing probe for immunoassay and genetic bioanalysis [24,134]. Furthermore, the same

group reported a photothermal biosensing platform for genetic detection employing AuNPs as the photothermal probe [27]. As illustrated in Fig. 3C, the hybridization between target DNAs and single-stranded DNAs (ssDNAs) led to the aggregation of AuNPs, accompanied by changes in the photothermal effect in the NIR light region as well as color changes. In this way, the genetic bioassay signals were simply recorded by a thermometer. In addition, Tang and co-workers also presented multiple photothermal immunoassays using different photothermal probes and contributed significantly to this field, such as $Cu_{2-x}Ag_xS$ NPs and Ti_3C_2 MXene QDs [133,135,136]. Other nanomaterials like GO and $Cu_{2-x}S$ were also reported as photothermal biosensing probes [120,137].

3.2.2. Signal amplification

To enhance the detection sensitivity, signal amplification is necessary for many biosensors, especially optical and electrochemical ones [110,138]. In this step, nanomaterials are mainly used to promote the signaling properties of their own or other relevant probes. Exploiting catalytic activities of nanomaterials, such as the peroxidase-mimic activity, is a representative sample in POC colorimetric bioanalysis [139,140]. Stevens and co-works developed an interesting lateral flow immunoassay (LFIA) using porous Pt core-shell nanocatalysts (PtNCs) to amplify the colorimetric signal [141], as diagramed in Fig. 4A. In the LFIA strip, the immunocaptured PtNCs with strong peroxidase-like activity catalyzed the oxidation of CN/DAB (4-chloro-1-naphthol/3,3'-diaminobenzidine, tetrahydrochloride), which significantly improved the sensitivity in colorimetric detection of an HIV biomarker (i.e., p24). Xia and colleagues reported a method to synthesize Pt-decorated AuNPs and used them as an immunochromatographic probe for PSA detection (Fig. 4B) [142]. Owing to the high peroxidase-like activity of the ultrathin Pt layers in the nanocomposites using TMB as the chromogenic substrate, it was proved that the immunoassay sensitivity was amplified by ~100 times compared with that of conventional AuNPs. Park et al. synthesized Au–Ag core-shell NPs *via* an in-situ growth route [143]. The loading of Ag nanoshells improved the peroxidase-like activity of the nanohybrids in the colorimetric detection of norovirus. Interestingly, Li's group exploited the peroxidase-like activity of Fe_3O_4 NPs in photothermal immunoassay using $_{ox}$TMB as the photothermal biosensing probe [24], accompanied with color changes to blue, as shown in Fig. 4C. The catalytic properties of Fe_3O_4 NPs amplified the photothermal signal and achieved a LOD of 1.0 ng/mL PSA using a common thermometer, which was comparable to some traditional ELISA methods using an expensive microplate reader.

Some nanomaterials exhibit remarkable electrochemical properties such as fast electron transportation and electrocatalytic activities, and are widely selected for signal amplification in electrochemical biosensors [144,145]. Zhang and co-workers proposed a sensitive electrochemical platform for DNA detection based on signal amplification by DNA-templated AgNPs [146]. In combination with the electrochemical atom transfer radical polymerization (eATRP), AgNPs were deposited in the genetic analysis system through a DNA templating process. Due to the excellent electrochemical properties of AgNPs, it was demonstrated that the detection performance was significantly amplified with a LOD as low as 4.7 aM. Escosura-Muñiz et al. synthesized bimetallic palladium (Pd)-AuNPs and studied the effect of Pd/Au composition ratio on their electrocatalytic activity toward the oxygen reduction reaction (ORR) [147]. By adjusting the ratio, the electrocatalytic activity was optimized and utilized for electrochemical immunosensing of hyaluronidase wound infection biomarkers. Electrochemical biosensors utilizing other nanomaterials, such as carbon-based nanomaterials and PtNPs, to amplify the detection signals have also been reported [148,149].

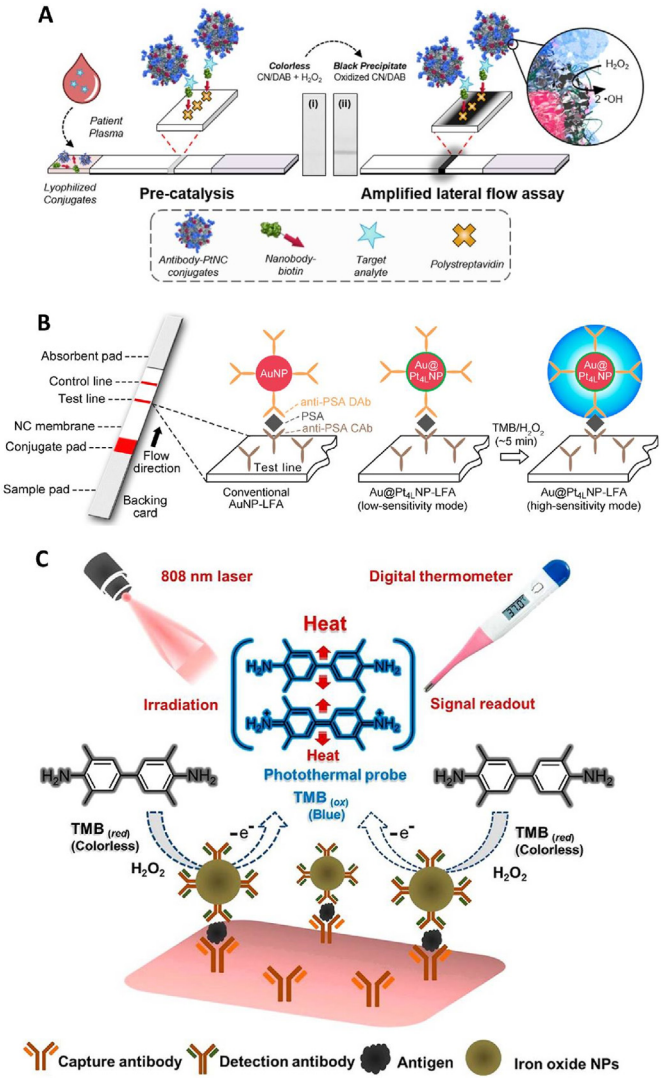

Fig. 4. Schemes of colorimetric and photothermal signal amplification using peroxidase-mimic activities and photothermal effects of nanomaterials. (A) LFIA using PtNCs to amplify colorimetric signals for p24 antigen detection. Adapted with permission from Ref. [141]. Copyright 2018 American Chemical Society. (B) LFIA using Pt-decorated AuNPs for colorimetric PSA detection. Adapted with permission from Ref. [142]. Copyright 2017 American Chemical Society. (C) Photothermal immunoassay of PSA using Fe_3O_4 NPs catalyzed-$_{ox}$TMB as photothermal biosensing probe. Adapted with permission from Ref. [24]. Copyright 2018 American Chemical Society.

Additionally, nanomaterials are widely utilized to enrich the signal labels (e.g., enzymes, nucleic acids, secondary antibodies, other nanomaterials or probes) to amplify the detection signals [150,151]. Taking advantage of the high surface-to-volume ratio of nanomaterials, a large number of chemical or biomolecular anchors (e.g., aptamers) can be immobilized on the surfaces of nanomaterials to amplify the molecule-recognition events in biosensors. For example, Zhang et al. reported an electrochemical immunosensor for PSA detection using AuNPs as the carriers of specific aptamers and signal probes (i.e., methylene blue) [152]. The aptamer-AuNP-signal probe (AASp) bioconjugates were captured in a sandwich-type immunosensing system, which were demonstrated to show a significant role in amplifying the detection signal utilizing square wave voltammetry (SWV). PSA was detected at a low LOD of 3.0 pg/mL with a linear concentration range of 0.001–75.0 ng/mL. Magnetic NPs with the modification of specific

ligands have been extensively exploited for target enrichment in pathogen detection [153]. Song and co-workers developed a fluorescent bioassay for the detection of *Staphylococcus aureus* (SA) using aptamer-coated magnetic beads (Apt-MBs) and vancomycin-stabilized Au nanoclusters (AuNCs@Van) [154]. Apt-MBs were employed to specifically enrich SA with the aid of an external magnet, followed by the fluorescent quantification of enriched SA by AuNCs@Van. SA was tested at a LOD of 16 CFU/mL.

3.2.3. Signal quenching

Nanomaterial-involved signal quenching is a popular strategy in fluorescent biosensors [110,155]. Because of the overlapping emission bands of fluorescent probes and absorption bands of nanomaterials as quenchers, quenching or recovery of fluorescence signals can be associated with molecule-recognition events [110,156]. In particular, FRET is an extensively used approach, where the quenchers also serve as fluorescent probes after accepting the transferred energy from the donors. To achieve effective quenching and recovery, the donors and acceptors should be sufficiently close in the spatial distance (i.e., 1–10 nm) [110,114].

Nobel metal NPs and carbon-based nanomaterials are well-known fluorescence quenchers ascribed to their optical absorption characters in a broad light window. Dai et al. developed a fluorescent biosensor for chlorothalonil (CHL) detection based on an inner-filter effect between AuNPs and ratiometric fluorescent QDs (RF-QDs) [96]. AuNPs functioned as a quencher of green fluorescence of RF-QDs. The dispersity of AuNPs was modulated by CHL-controlled papain (PAP) activity, through which the fluorescence was quenched or restored. Mirzaee and co-workers established a sensitive fluorescent biosensor for the determination of microRNAs utilizing AgNPs as the fluorescence quencher of La(III)-modified metal-organic frameworks (MOFs) [157]. In the presence of target microRNAs, hybridization-induced linking between La(III)-MOFs and AgNPs caused the fluorescence quenching in the system. Additionally, Ju et al. reported a fluorescent method for testing mycoplasma pneumoniae (MP) based on the interaction between tetrapod G-quadruplex (TP-G4) and GO [158]. GO worked as a fluorescence quencher of TP-G4, which was initially adsorbed on the surface of GO. The specific recognition of target MP with TP-G4 resulted in the detachment of the fluorophore from GO along with the recovery of the fluorescence signal. Yoon's group presented a simple and cost-effective LFIA to test cardiac troponin I (cTnI) using a time-resolved FRET technique [159]. In the LFIA strip, europium (Eu)-chelate silica (Eu–Si) NPs were used as the fluorescence donor, while antibody-conjugated Au nanorods acted as the fluorescence acceptor. Taking advantage of the FRET approach, cTnI was evaluated at a LOD as low as 97 pg/mL in human serum.

4. Application of nanosensor-integrated microfluidic platforms for POC bioanalysis

Microfluidics offers a powerful LOC platform for POC bioanalysis with the integration of nano-biosensors. Employing microfabrication techniques and microelectromechanical systems (MEMSs), arrays of nano-biosensors can be integrated into microfluidic devices, which serve as a versatile and more precise toolbox for monitoring the analytical performance of nano-biosensors in microscale environments [110]. Thanks to the microfluidic integration, nano-biosensors also find an excellent platform to better play their roles in POC bioanalysis. Various kinds of microfluidic nano-biosensors integrated with various nanomaterials-related detection methods, including colorimetry, fluorescence, electrochemistry, electrochemiluminescence, and new detection methods such as distance-based and photothermal biosensing (i.e. photothermometric) detection methods have been developed for POC testing of a wide range of biomolecules [110,160], as discussed in this following sections. The combination of the microfluidic technology with nano-biosensors are opening new opportunities in POC bioanalysis. In this section, we highlight recent advances in the working principles of these microfluidic nano-biosensors.

4.1. Colorimetric detection

Colorimetric assay is one of the most widely used detection methods in nano-sensor-based microfluidic platforms, which is based on the changes in colors caused by chemical reactions between nano-sensors and the analytes [161,162]. Integration of colorimetric detection methods on microfluidic devices attracted lots of attention because colorimetric assays on chips do not need bulky off-chip detection systems; therefore, naked-eye–based readouts can be obtained [16].

Many researchers have applied the colorimetric detection method by integrating nano-sensors on polymer-based microfluidic platforms to develop bioanalysis techniques. For example, Chen et al. developed a portable visual quantitative device for Creatine kinase MB (CK-MB) by incorporating target-responsive DNA hydrogel with a PMMA microfluidic chip [163]. The CK-MB aptamer and the complementary short DNA strand were separately grafted onto the polyacrylamide strand and formed the hydrogel by base-paired linkage. Upon the presence of CK-MB, the aptamer bounded to CK-MB. This led to hydrogel dissociation and subsequent release of pre-trapped AuNPs, which was proportional to the concentration of CK-MB. The hydrogel was combined with a microfluidic chip to achieve portable on-site detection. The color change caused by the released AuNPs was evaluated by taking a picture and analyzing the average gray values. The average gray values were linearly related to the CK-MB concentration in the range of 0.2–625 nM, and as low as 0.027 nM CK-MB could be detected by cell phone. The recoveries of the microfluidic method for the determination of CK-MB in serum ranged from 96.63% to 106.25%, with the RSDs less than 5%. Man et al. presented a microfluidic colorimetric biosensor for detecting *Salmonella* using thiolated polystyrene microspheres (SH-PSs) for aggregating AuNPs, and smartphone imaging software for monitoring colorimetric signals [164]. The structural diagram of the designed microfluidic chip is shown in Fig. 5A (a). Complementary DNA-magnetic nanoparticle (cDNA-MNP) conjugates were used as capture probes and reacted with the free aptamer-PS-cysteamine conjugates. As shown in Fig. 5A (b), AuNPs were aggregated on the surface of *Salmonella*-aptamer-PS-cysteamine conjugates, resulting in a visible color change in the detection chamber, indicating different concentrations of *Salmonella*. The detection limit was as low as 60 CFU/mL, and the linear range was from 60 to 6.0×10^5 CFU/mL (Fig. 5A (c-d)). The microfluidic biosensor was evaluated by analyzing salad samples spiked with *Salmonella*. The recoveries ranged from 91.68% to 113.76%, which indicated its potential application in real samples. In addition, Qi and coworkers introduced a microfluidic biosensor using metal-organic framework NH_2-MIL-101(Fe) for determination of *Salmonella* in chicken meat samples with a lower LOD of 14 CFU/mL [165]. The colorless o-phenylenediamine and H_2O_2 were catalyzed by using the MOF complexes to generate yellow 2,3-diaminophenazine (DAP). The experimental results showed that the biosensor could detect *Salmonella* from 1.5×10^1 to 1.5×10^7 CFU/mL in 1 h. The mean recovery for *Salmonella* in spiked chicken meats was abut 112%. Hu et al. proposed a DNA colorimetric multilevel circuit construction strategy using AuNPs as an indicator without any modification and labeling steps [166]. Two colorimetric logic gates were constructed based on the aggregation of AuNPs mediated by molecular recognition between DNA and protoberberines (palmatine/berberine).

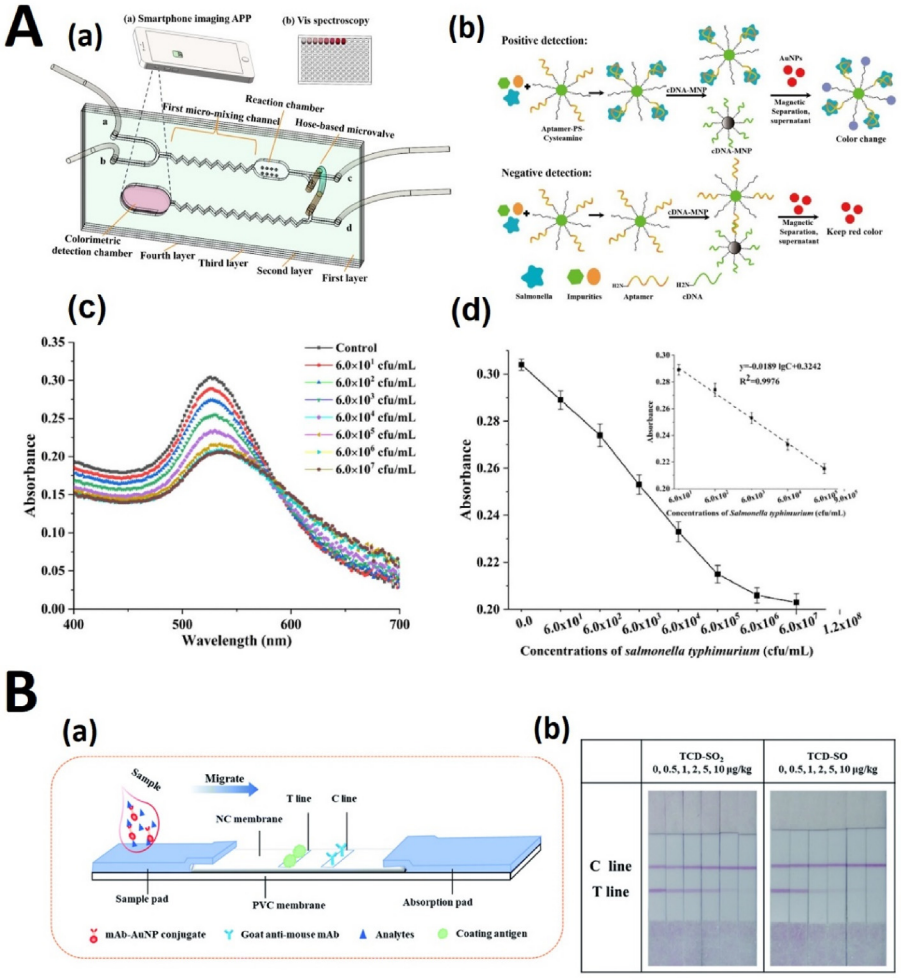

Fig. 5. Nanomaterial-based microfluidic platforms for POC colorimetric bioanalysis. (A) 3D structure of a microfluidic chip for detecting *Salmonella typhimurium* based on SH-PSs, hose-based microvalve, and smartphone imaging APP (a); and the detection strategy of the microfluidic colorimetric biosensor by using SH-PSs to aggregate AuNPs for the detection of *Salmonella typhimurium* (b). (c) The visible absorption spectrum of the AuNPs solution with different concentrations of *Salmonella typhimurium*; (d) Absorbance of the AuNPs solution versus the concentrations of *Salmonella typhimurium* and the linear correlation between absorbance of AuNPs solution in the colorimetric detection chamber and *Salmonella typhimurium* concentrations. Adapted with permission from Ref. [164]. Copyright 2021 Elsevier. (B) Schematic of an AuNP-based lateral flow assay for detection of TCD and its metabolites (a); and qualitative testing results of TCD-SO and TCD-SO_2 in bovine muscle samples with the test strips (b). Adapted with permission from Ref. [172]. Copyright 2019 The Royal Society of Chemistry.

The LOD of the PMMA-based microfluidic device for the detection of *Streptomyces* sp. DNA was 0.25 μg/mL by naked eyes within 10 min. A linear relationship ($R^2 = 0.99$) was achieved between the A670/A520 and DNA concentrations from 0.1 μg/mL to 0.6 μg/mL.

Microfluidic paper-based analytical devices combined with nano-sensor-based colorimetric detection have aroused wide attention. For instance, Luan et al. integrated a Cerium metal-organic framework (Ce-MOF) in the origami paper Slip-Chip to directly detect glucose and uric acid levels in serum without sample handling or extra analytical equipment except for a smartphone [167]. The LODs were 0.069 mM and 39.6 M for glucose and uric acid, respectively. 55 clinical samples (22 from diabetic and 33 from healthy adults) for glucose detection and 46 clinical samples (20 from patients with hyperuricemia and 26 from healthy adults) for uric acid detection were tested. The interclass correlation coefficient (ICC) and Bland-Altman analysis were employed to evaluate the agreement between the presented device and the clinical blood test. The ICC was 0.867 and 0.933 for glucose and uric acid analysis, respectively. The achieved ICC showed the device had great consistency with the clinical blood test. Pinheiro et al. applied chemically produced and tailored AuNPs in paper-based microfluidic platforms to measure three relevant health markers, free cholesterol, glucose, and uric acid [168]. Two steps were applied to perform the assays. First, the direct effect of the target analyte caused the reduction of the gold salt, influencing the plasmonic properties of resulting AuNPs. And then, tailoring the plasmonic properties of functionalized AuNPs by etching or aggregation effects when the target analytes bond with the functionalizing agents, resulted in varying color signals. The calibration curve for glucose was linear from 1.25 to 20 mM, and the lowest detectable concentration of glucose was 1.25 mM. The LODs of uric acid were 71 μM and 81 μM based on the R/B and hue calibration metrics, respectively. As low as 81 μM cholesterol was detected. However, the obtained LOD for the detection of glucose is higher than the reported LOD by Luan et al., but the reported LOD for uric acid detection was much lower than the reported LOD by Luan et al. [167]. Alizadeh et al. reported a paper-based analytical device combined with Co_3O_4–CeO_2 nanosheets for colorimetric-based detection of glucose [169]. The Co_3O_4–CeO_2 nanocomposite in the presence of glucose oxidase enzyme was utilized for glucose

detection using paper as a measuring platform. The color change of the platform was recorded using a mobile camera and analyzed by a smartphone application. The nano-sensor presented quantification of glucose in the concentration range of 0.005–1.5 mM with a LOD of 0.21 μM which was much lower than the achieved LODs of glucose detection in the previously explained papers [167,168]. The application of the proposed assay for colorimetric measurement of glucose in human serum samples was evaluated with satisfactory results and %RSD between 2.69% and 4.74%. Recently, Li and co-workers reported a low-cost and disposable paper-based immunosensor for instrument-free colorimetric detection of pancreatic cancer biomarker PEAK1 (pseudopodium-enriched atypical kinase one, SGK269) by capitalizing the catalytic properties of AuNPs in color dye degradation [28]. The signal amplification method increased the detection sensitivity by about 10-fold. The LOD of 1 ng/mL PEAK1 was obtained and the calibration curve presented a linear range between 1 and 10^4 ng/mL PEAK1, with a squared correlation coefficient of 0.975. Liu et al. developed water-soluble molybdenum oxide quantum dots (MoOx QDs) as highly effective biomimetic catalysts prepared by a facile ultrasonic-assisted hydrothermal method [170]. The MoOx QDs displayed peroxidase-like activity and were constructed for efficient colorimetric quantitative detection of H_2O_2 based on a microfluidic paper-based device. As low as 0.175 μmol/L H_2O_2 was determined with a linear range from 1 to 20 μmol/L. Moreover, this biosensing device was successfully applied for the visual detection of H_2O_2 released from PC12 cells. The recoveries were obtained in the range of 91.5–107.04%.

The lateral flow strips integrated with nano-sensors are widely developed as desirable POC bioanalysis tools because of their easy and fast self-diagnostic characteristics. For example, Xu and Li et al. reported a smartphone-based on-site nucleic acid testing (NAT) platform that could image and analyze lateral flow nucleic acid assays in POC settings [171]. An inexpensive add-on was developed to run lateral flow assays while providing homogeneous ambient light for imaging. Moreover, an Android app with a user-friendly interface was designed for the result analysis and management. A relationship function between nucleic acid concentrations and the colorimetric reaction was established and evaluated by leave-one-out cross validation. The result showed the true value and the predicted value had a high agreement with an R-square value of 0.96. Wang et al. reported a monoclonal antibody (mAb)-based LFIA for the rapid screening of triclabendazole (TCD) and its metabolites in foodstuff using gold nanoparticles as a label [172]. As shown in Fig. 5B (a), a sample pad, absorption pad, nitrocellulose (NC) membrane, and polyvinyl chloride (PVC) backing card were the main constituents of the test strip. Under optimized conditions, the LODs were 0.11 μg/kg for TCD, 0.28 μg/kg for TCD-SO, 0.38 μg/kg for TCD-SO_2, and 0.47 μg/kg for Keto-TCD (Fig. 5B (b)). The ranges of quantitative detection were 0.22–5.41 μg/kg for TCD, 0.56–5.74 μg/kg for TCD-SO, 0.76–9.11 μg/kg for TCD-SO_2, and 0.94–24.02 μg/kg for Keto-TCD, respectively. Finally, the assay was applied to detect TCD and its metabolites in bovine muscle samples, and the recoveries ranged from 92.0 to 107.0% for TCD, 93.1–102.0% for TCD-SO, 96.3–101.2% for TCD-SO_2, and 95.7–107.3% for Keto-TCD, respectively. Dalirirad et al. designed an aptamer-based lateral flow strip assay for rapid on-site detection of cortisol in sweat [173]. Cortisol in sweat has been identified as a key biomarker for monitoring physiological stress. The nano-sensor-based microfluidic device was developed by conjugating cortisol-selective aptamers to the surface of AuNPs. The device enabled the visual detection of cortisol in 5 min. The device exhibited a visual limit of detection of 1 ng/mL cortisol, readily covering the normal range of free cortisol in sweat (8–140 ng/mL). To evaluate the stability of the device, the strips were stored in sealed plastic bags, kept at 4 °C for 1–10 days, and then used for cortisol detection. The results of subsequent tests were nearly the same for all samples. In addition, Akkapinyo et al. fabricated a multiplex hepatitis B test paper strip to serve as a rapid test for hepatitis B screening [174]. It was developed to simultaneously assess three essential serological markers of hepatitis B virus infection, including hepatitis B surface antigen (HBsAg), hepatitis B surface antibody (Anti-HBs), and hepatitis B core antibody (Anti-HBc). AuNPs were utilized as the signal generator on the test strip. Furthermore, a part of a paper network was incorporated into the strip for the gold-silver enhancement process. The detection limits of HBsAg, Anti-HBs, and Anti-HBc were obtained at 0.5, 0.3, and 0.1 μg/mL, respectively. However, the detection sensitivity was not very high, and the Li group achieved much lower LODs for colorimetric detection of HBsAg using two polymer/paper hybrid microfluidic devices [25,175].

Li and co-workers recently developed a paper/polymer microfluidic platform integrated with gold nanorods (AuNRs) based multicolorimetric ELISA biosensors for colorimetric POC detection of infectious diseases [22]. The multicolormetric ELISA platform was built on multiple distinct color variants resulted from the catalytic oxidation of 3,3',5,5'-tetramethylbenzidine (TMB) and the etching of AuNRs. The vivid color changes could be easily recognized by the naked eye, and their red mean values allowed quantitative biomarker detection, without using any specific instruments. When the multicolorimetric ELISA was integrated on a paper/PMMA hybrid analytical platform, it not only provided integrated processing and high portability but also enabled fast assays in about 50 min. The limit of detection of 9.1 ng/mL of the hepatitis C virus core antigen (HCVcAg) was obtained using the presented multicolorimetric ELISA platform.

Most colorimetric labels used in microfluidic devices are metallic nanoparticles, but non-metallic nanoparticles recently attracted attention for colorimetric-based microfluidic chips for bioassays. For example, Alizadeh et al. developed a sensing system based on the non-oxidation reduction strategy using polymer nanocomposite film (PNF) as a probe for direct detection of ascorbic acid (AA) through a colorimetric method [176]. The color of the PNF nanoprobe was turned from purple to colorless for the detection of AA. The absorbance at 604 nm was linearly related to the logarithm of the AA concentration in the range of 50–425 μM with a LOD of 10 μM. Moreover, a droplet-based PDMS/glass microfluidic platform was developed for intracellular imaging of AA in living cells [176]. Isolated small microdroplets allowed the detection and imaging of AA in single cells. Zhang et al. developed a wearable PDMS microneedle colorimetric patch integrating the sampling function and the capability of real-time uric acid (UA) analysis in a minimally invasive manner [177]. To operate the constructed device, the poly(vinyl alcohol) based microneedle was embedded with the uricase, which catalyzed the oxidation of UA extracted from the interstitial fluids and produced H_2O_2. Polypyrrole nanoparticles (PPy NPs) with peroxidase-like activities encapsulated in the display layer triggered the reaction between H_2O_2 and TMB, resulting in color variations associated with the concentration of H_2O_2 produced by the UA oxidation. Thus, the UA level was determined with the naked eye. According to the relationship between the color intensity and the UA concentration, the UA level within 200–1000 μM was quantified by analyzing sample images with a smart phone. The developed device exhibited a LOD of about 65 μM.

Colorimetric methods are user-friendly because of their simple operation and visual readout of results using the naked eye without the need for any specific equipment; however, these techniques are suffered by low sensitivity and limited quantification capbility [178]. Therefore, some researchers have devoted efforts to improving the quantitative ability of colorimetric-based microfluidic platforms. For instance, Tong et al. developed an artificial

intelligent (AI)-assisted colorimetric polydopamine nanoparticle (PDA)-based LFIA platform for the quantification of neutralizing antibodies produced from vaccinations [179]. The platform integrated PDA-based LFIA and a smartphone-based reader to test the neutralizing antibodies in serum, where an AI algorithm was also developed to analyze the results quantitatively. The developed platform achieved quantitative detection with the LOD of 160 ng/mL of and the detection range of 625–10000 ng/mL. Celik et al. used anthocyanins from red cabbage (*Brassica oleracea*) as a natural pH indicator and incorporated it into a colorimetric strategy for the detection of *Helicobacter pylori* (*H. pylori*) (RCE@test) [180]. Two sets of RCE@test solutions (test 1 was purple, and test 2 was blue) were prepared in different forms, including liquid, adsorbed filter paper, and agar. The performance of each RCE@test was investigated as a function of the test volume, the *H. pylori* concentration, and the reaction time. To elucidate the effect of the pathophysiological environment on the RCE@tests, *H. pylori* in an artificial gastric fluid was also detected. Two *H. pylori* suspensions (10 and 1 CFU/mL) were detected in 15 min and 3 h, respectively, and the LOD was determined down to 1 CFU/mL.

4.2. Fluorescence and chemiluminescence detections

Fluorescence is widely used as an optical technique for bioanalysis in nano-sensor-based microfluidic chips due to highly sensitive and selective fluorescent labeling techniques. Recently, carbon-based nanoparticles were widely integrated on microfluidic devices for fluorescence based POC bioanalysis. For instance, Rossini et al. presented a multilayer paper device integrated with carbon dots for the analysis of saliva samples [181]. The proposed technique utilized the oxidation of glucose and lactate, catalyzed by specific oxidase enzymes, producing hydrogen peroxide. The detection was based on the fluorescence quenching of carbon dots in the presence of hydrogen peroxidase. The concentrations of the analytes showed good linear correlations with fluorescence quenching, with LODs of 2.6×10^{-6} and 8.1×10^{-7} mol/L for glucose and lactate, respectively. The proposed method presented satisfactory intra-day and inter-day repeatability, with %RSD values in the 3.8–6.6% range. The device was applied to saliva and serum samples and was validated using certified materials. The errors obtained for these determinations were lower than 7%, showing satisfactory precision of the proposed method. The concentrations obtained using the described method were compared with the certified concentrations using the *t*-test, which showed no significant differences between the concentrations, confirming the accuracy of the proposed method. The Li group reported an interfacial nanosensing strategy based on aptamer-functionalized GO nanosensors in PDMS microfluidic droplets for the high-sensitivity one-step detection of 17β-estradiol and other low-solubility molecules [182]. The LOD was found to be as low as 0.07 pM, while the LODs of most aptamer-based biosensors for estradiol were in the range of nM [183] or above the pM range [184]. The sensitivity of the droplet microfluidic nanosensing system was further compared with conventional off-chip methods by testing various concentrations of estradiol. The LODs of the conventional off-chip methods were 200-folds higher than that of the interfacial nano-biosensing system. In addition, the same group developed a PMMA/paper hybrid CD-like microfluidic device integrated with DNA probe-functionalized GO nanosensors for multiplex quantitative LAMP detection (mqLAMP) of multiple infectious diseases (Fig. 6A) [67]. Two PMMA layers were tightened by a screw in the center, allowing the rotation of one layer over the other when loosening the screw. The Cy3-labeled DNA capture probes were pre-loaded on the GO-functionalized paper disk, in which the fluorescence was quenched initially (Fig. 6A (b)). After LAMP reaction, the SpinChip was turned over and rotated to let the mLAMP microzone pass by different detection zones with paper disks inside. By using the device, two bacterial pathogens, *N. meningitidis*, and *S. pneumoniae*, were identified and quantified, with the LODs of 6 copies and 12 copies per assay, respectively.

The light transparency of PDMS makes PDMS-based microfluidic devices ideal for integrating nano-sensors on a chip for fluorescence-based bioanalysis. Numerous researchers presented PDMS-based microfluidic platforms for fluorescence-based nano-biosensing. For example, Wu et al. developed a PDMS-based microfluidic sensing platform using CuO nanoparticles for ultra-sensitive neuron-specific enolase (NSE) detection [185]. A strategy of catalytic oxidation of AA by CuO nanoparticles was proposed to initiate fluorescence signals. CuO nanoparticles growing on conductive carbon spheres (CuO@CSs) as secondary antibodies' labels could efficiently catalyze the oxidation of AA. Then, the produced dehydroascorbic acid reacting with o-phenylenediamine opportunely generated strong fluorescence signals. A wide linear range of 0.001–150 ng/mL and a low LOD of 0.25 pg/mL were achieved to detect NSE. The standard addition method was used to evaluate the potential feasibility of the proposed microfluidic biosensor in clinical applications by applying it to human serum samples. The RSD was less than 5%, and the recoveries were from 94.0 to 100.6%. Wang et al. developed a PDMS microfluidic biosensor for online and sensitive detection of *Salmonella typhimurium* (*S. Typhimurium*) based on immunomagnetic separation, fluorescence labeling, and smartphone video processing [186]. First, the immune magnetic nanoparticles were used to separate and efficiently concentrate the target bacteria specifically, and the magnetic bacteria were formed. Then, the magnetic bacteria were labeled with the immune fluorescent microspheres, and the fluorescent bacteria were formed. Finally, the fluorescent bacteria were continuously injected into the microfluidic chip on the smartphone-based fluorescent microscopic system. The fluorescent spots were counted online using the smartphone software based on inter-frame difference algorithm to obtain the amount of the target bacteria. Under the optimal conditions, the proposed microfluidic device could quantitatively detect *S. Typhimurium* ranging from 1.4×10^2 to 1.4×10^6 CFU/mL, and its lower detection limit was 58 CFU/mL. Spiked apple juice samples were analyzed using the device to further evaluate the applicability of the proposed nano-sensor-based microfluidic platform for testing Salmonella in real samples. The recoveries for different concentrations of *S. Typhimurium* in apple juice ranged from 84.82% to 98.39%, with an average recovery of 92.64%. Huang et al. proposed an acid-responsive PDMS microfluidic biosensor using curcumin (CUR) and ZnO-capped mesoporous silica nanoparticles (MS NPs) for the detection of *S. Typhimurium* in fluorescent modal [187]. As shown in Fig. 6B (a), the MSNs were first incubated with CUR to obtain MSN@CUR nanoparticles (MC NPs). The MC NPs were then capped with ZnO nanoparticles to form MSN@CUR@ZnO nanoparticles (MCZ NPs) to prevent CUR from premature release, followed by modification with polyclonal antibodies (pAbs) against *S. Typhimurium* to obtain immune MCZP NPs. The immune magnetic nanoparticles (MNPs), the *S. Typhimurium* cells, and the MCZP NPs were conjugated in the microfluidic chip with a Koch fractal mixing channel to form MNP-bacteria-MCZP complexes (Fig. 6B (b)). Finally, acetic acid (HAc) was introduced to release CUR from the complexes, and fluorescence changes were measured to determine the concentration of *S. Typhimurium*. This proposed biosensor was able to quantitatively detect *S. Typhimurium* ranging from 10^2 to 10^7 CFU/mL in 1.5 h and the lower detection limits were calculated to be 40 CFU/mL. The mean recovery was about 104% for *S. Typhimurium* in the spiked chicken samples. The sensitivity of the presented approach was better than the device presented by Wang

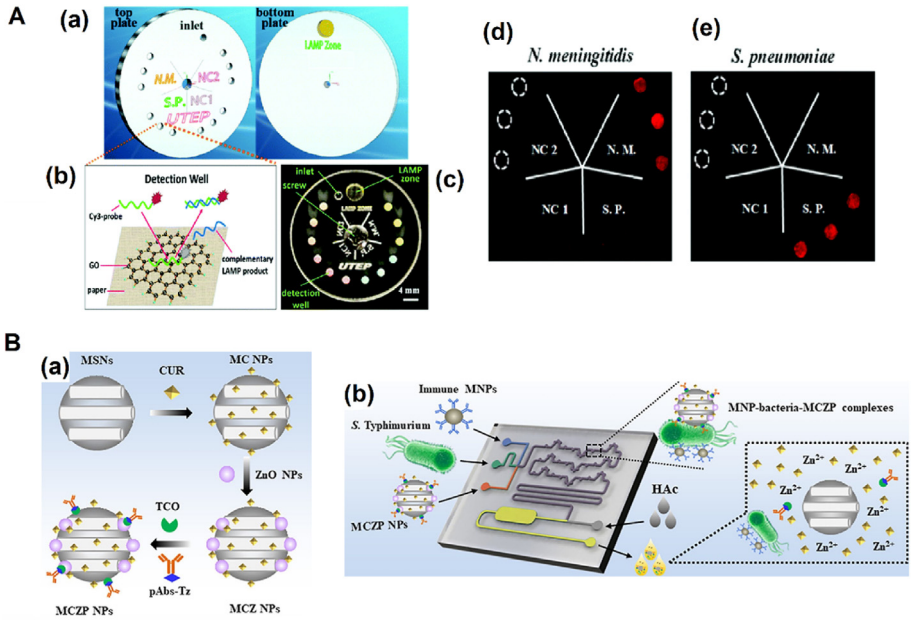

Fig. 6. Microfluidic platforms integrated with nano-sensors for fluorescence-based POC bioanalysis. (A) Schematic of the PMMA/paper hybrid microfluidic SpinChip for mqLAMP detection. (a) 3D schematic of the exploded view of the SpinChip. (b) Detection principle based on the interaction among the GO, ssDNA probes, and target LAMP products. (c) A photograph of the assembled PMMA/paper hybrid microfluidic SpinChip. Fluorescence images of nanosensor microzones after recovery for specificity investigation by testing *N. meningitidis* (d) and *S. pneumoniae* (e) samples with their corresponding and non-corresponding ssDNA probes. Adapted with permission from Ref. [67]. Copyright 2017 The Royal Society of Chemistry. (B) Schematic of preparing immune MSN@CUR@ZnO@pAbs nanoparticles (MCZP NPs) (a); and schematic of the proposed microfluidic biosensor for rapid and sensitive detection of *S. Typhimurium* (b). Adapted with permission from Ref. [187]. Copyright 2020 Elsevier.

et al. [186] for detection of *S. Typhimurium*.

Compared to colorimetric detection, one of the drawbacks of fluorescence detection is that a fluorescence optical detection system is complex and bulky. To address this, the Li group presented several POC microfluidic devices based on fluorescence instrument-free detection of infectious diseases without the need for any bulky and expensive equipment [19,68,83,188], in which generated fluorescence can be observed by the naked eye or taken an image with a smartphone camera. For instance, LAMP was integrated with polymer/paper hybrid microfluidic biochips for instrument-free detection of pathogens with high sensitivity and specificity [19,68,188], in which calcein was used as the fluorescence probe. Results could be visually observed by the naked eye or imaged by a smartphone camera under a portable UV light source. Without using any specialized laboratory instrument, the LODs of a few DNA copies per LAMP zone for pathogens were achieved within 1 h.

Chemiluminescence (CL) is another optical detection technique for bioanalysis that is more convenient for POC setting because this technique does not need an excitation light source and emission filters, compared to fluorescence detection. Several nano-sensor-based microfluidic platforms were developed for bioanalysis based on chemiluminescence detection. For instance, Zong et al. proposed an immunoassay for the detection of C-reactive protein (CRP), an important cerebrovascular disease marker, by a combination of metal-enhanced chemiluminescence (MEC) signal tag with a glass immunosensor chip (Fig. 7A) [189]. Two kinds of AgNP probes, DNA-hemin/DNA-A/biotin-DNA modified AgNPs (Probe A) and DNA-hemin/DNA-B modified AgNPs (Probe B), were prepared. The MEC signal tag was formed by the Probe A and Probe B link through the hybridization of DNA-A and DNA-B. The formed AgNP hybrid probes brought excellent CL signal amplification, due to the increased content of hemin molecules and the great MEC effect. The AgNP hybrid probes can be bound to the biotinylated antibody of sandwich immunocomplex for the immunoassay of CRP. Under optimal conditions, the method showed a wide detection range of 7×10^{-7} to 0.07 mg/mL and a LOD down to 0.05 ng/mL. The relative errors of detection of different concentrations of CRP in clinical serum samples were less than 4.94%. Cui and co-workers [190] achieved simultaneous determination of three acute myocardial infarction (AMI) biomarkers by a 3D μPAD with temporally resolved CL emissions (Fig. 7B). A dual-signal amplification strategy was introduced, employing primary antibody functionalized gold nanoparticles (Ab_1-GNPs) immobilized on the detection zone as amplified capture probes, and Co(II) catalyst, secondary antibody, luminol multifunctionalized gold nanoparticles (Co(II)-Ab_2-luminol-GNPs) with excellent CL activity as amplified signal probes. CL immunoreactions were performed at three detection zone of the fabricated 3D μPAD by assembling Ab1-GNPs, antigen, and Co(II)-Ab_2-luminol-GNPs to form sandwich-type immunocomplexes. Auto-separated CL signals with a temporal resolution were obtained by time-delayed transport of H_2O_2 to different detection zones for multiplexed analysis. Three AMI biomarkers, including heart-type fatty acid-binding protein (H-FABP), cardiac troponin I (cTnI), and copeptin, were analyzed in one CL detection run by reading the CL intensity of the obtained three CL emission peaks. The detection range were ultra-wide ranged from 0.1 pg/mL to 1 μg/mL, 0.5 pg/mL to 1 μg/mL, and 1 pg/mL to 1 mg/mL with the LODs down to 0.06 pg/mL, 0.3 pg/mL, and 0.4 pg/mL for H-FABP, cTnI, and copeptin detection, respectively.

To provide readers a better overview of current advances in microfluidic nano-biosensors with optical detection methods, we summarized most work in the field with colorimetric, fluorescence, and chemiluminescence detection, in Table 1.

4.3. Electrochemical detections

Electrochemistry has emerged as one of the most popular analytical methods in microfluidic devices, attributed to the high sensitivity, good selectivity, and ease of miniaturization of the

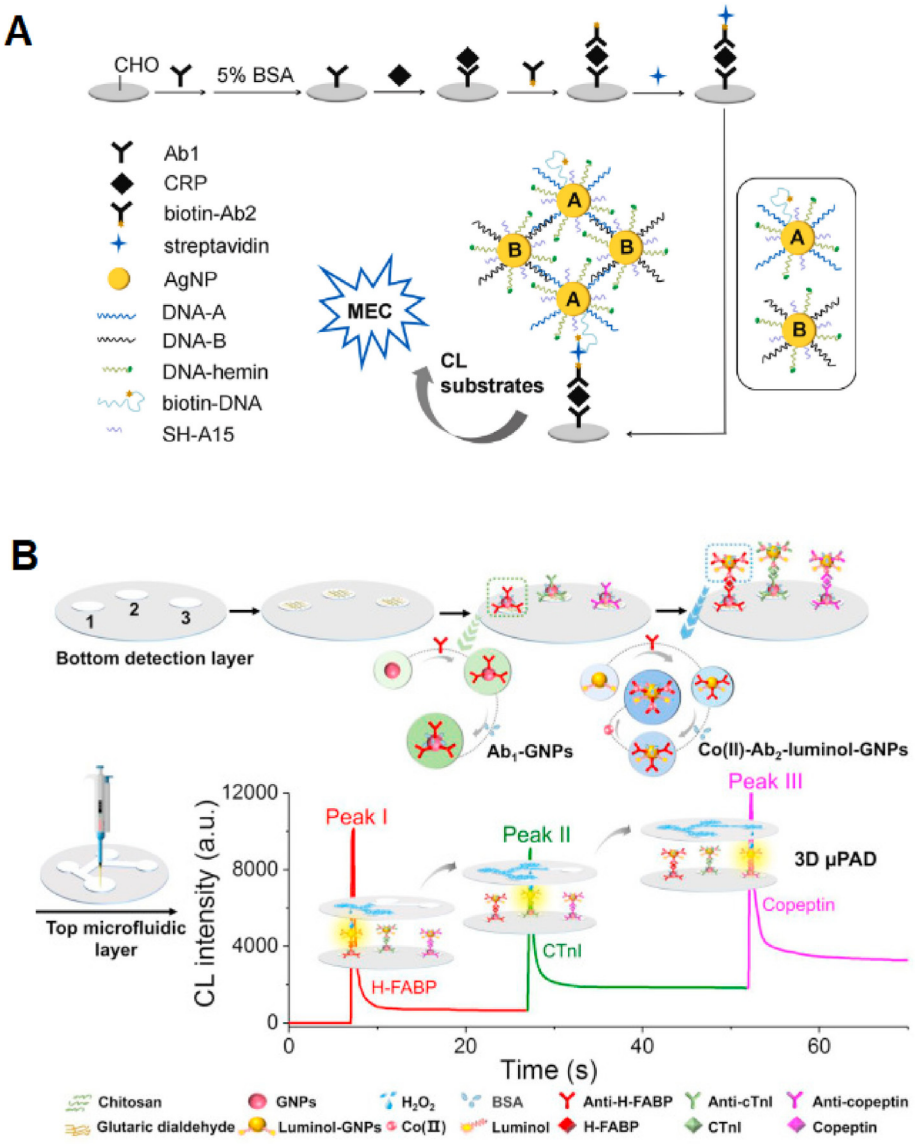

Fig. 7. Microfluidic nano-sensors for chemiluminescence based bioanalysis. (A) Schematic diagram of the procedure of the MEC immunoassay for detection of CRP based on AgNP hybrid probes. Adapted with permission from Ref. [189]. Copyright 2019 Elsevier. (B) Schematical illustration for the fabrication of the 3D μPAD for multiplexed CL immunoassay of H-FABP, cTnI and copeptin. Adapted with permission from Ref. [190]. Copyright 2020 Elsevier.

detection settings [191]. It has been a mature route to fabricate the three-electrode system in chambers or even micro-channels of microfluidic chips *via* techniques such as screen printing, inkjet printing, and electronic sputtering [26,192]. Nanomaterials can participate in signal transduction and amplification in electrochemical microfluidic biosensors like conventional ones. In the signal readout, microfluidic devices can be assembled with electrochemical measurement circuits or interfaced with external working stations.

μPADs have become an excellent choice for developing electrochemical nano-biosensors since electrodes can be easily deposited on paper substrates *via* the screen printing technique [191–193]. Liu and co-workers reported a paper-based electrochemical impedance spectroscopy (EIS) nano-biosensor for detecting p24 antigen (a biomarker of HIV) and IgG antibody (i.e., CR3022) to severe acute respiratory syndrome coronavirus 2 (SARS-CoV-2) [194]. A hydrothermal method was employed to grow zinc oxide nanowires (ZnO NWs) on carbon ink-deposited working electrodes (WEs). It was demonstrated that ZnO NWs decreased the electrical resistance of WEs and ensured reliable EIS analytical results. The microfluidic nano-biosensor can detect P24 antigen at a LOD of 0.4 pg/mL and distinguish varying concentrations of the CR3022 antibody (specific to SARS-CoV-2 spike glycoprotein S1) from 10 ng/mL to 1 μg/mL in spiked human serum samples. Li et al. developed a paper-based microfluidic electrochemical immunosensor for quantitative detection of PEAK1 as a new biomarker of pancreatic cancer [193], as shown in Fig. 8A. GO and AuNPs were employed as the hosts for immobilizing capture antibody and electrochemical probes to label the detection antibody, respectively. PEAK1 was detected at a low LOD of 10 pg/mL with a broad linear range of 10–10^6 pg/mL employing differential pulse voltammetry (DPV), providing a more sensitive method for early detection of pancreatic cancer than a colorimetric method (LOD, 1 ng/mL). The recovery values ranged in a satisfactory criterion from 103% to 104% in testing of spiked human serum samples [28]. Cai et al. presented an origami-paper-based electrochemical

Table 1
Microfluidic nano-biosensors with colorimetric, fluorescence, and chemiluminescence detection.

Method	Device Substrate	Nanomaterial	Target	Linear Range	LOD	Ref.
Colorimetric	Paper	AuNPs	PEAK1	1–10^4 ng/mL	1 ng/mL	[28]
Colorimetric	PMMA	AuNPs	CK-MB	02–625 nM	0.027 nM	[163]
Colorimetric	NOA81	AuNPs	*S. Typhimurium*	60–6.0 × 10^5 CFU/mL	60 CFU/mL	[164]
Colorimetric	PDMS	NH_2-MIL-101 MOF	*S. Typhimurium*	15–1.5 × 10^7 CFU/mL	14 CFU/mL	[165]
Colorimetric	PMMA	AuNPs	*Streptomyces* sp.	0.1–0.6 μg/mL	0.25 μg/mL	[166]
Colorimetric	Paper	Ce-MOF	Glucose	–	0.069 mM	[167]
			Uric acid	–	39.6 mM	
Colorimetric	Paper	AuNPs	Cholesterol	–	81 mM	[168]
			Glucose	1.25–20 mM	1.25 mM	
			Uric acid	–	71 μM/81 μM	
Colorimetric	Paper	Co_3O_4–CeO_2	Glucose	0.005–1.5 mM	0.21 μM	[169]
Colorimetric	Paper	MoOx QDs	H_2O_2	1–20 μM	0.175 μM	[170]
Colorimetric	NC/PVC	AuNPs	HIV	2.5–200 nM	2.5 nM	[171]
Colorimetric	NC/PVC	AuNPs	TCD	0.22–5.41 μg/kg	0.11 μg/kg	[172]
			TCD-SO	0.56–5.74 μg/kg	0.28 μg/kg	
			TCD-SO_2	0.76–9.11 μg/kg	0.38 μg/kg	
			Keto-TCD	0.94–24.02 μg/kg	0.47 μg/kg	
Colorimetric	NC	AuNPs	Cortisol	8–140 ng/mL	1 ng/mL	[173]
Colorimetric	Paper	AuNPs	HBsAg	5–3000 ng/mL	0.5 μg/mL	[174]
			Anti-HBs	–	0.3 μg/mL	
			Anti-HBc	–	0.1 μg/mL	
Colorimetric	Paper/PMMA	AuNRs	HCVcAg	10–100 ng/mL	9.1 ng/mL	[22]
Colorimetric	PDMS/glass	PNF	Ascorbic acid	50–425 μM	10 μM	[176]
Colorimetric	PDMS	Polypyrrole NPs	Uric acid	200–1000 μM	65 μM	[177]
Colorimetric	NC/PVC	Polydopamine NPs	Neutralizing antibodies	625–10000 ng/mL	160 ng/mL	[179]
Fluorescence	Paper	CDs	Glucose	5–50 × 10^{-6} M	2.6 × 10^{-6} M	[181]
			Lactate	2.5–20 × 10^{-6} M	8.1 × 10^{-7} M	
Fluorescence	PDMS	GO	17β-estradiol	0.1–1000 pM	0.07 pM	[182]
Fluorescence	Paper/PMMA	GO	*N. meningitidis*	6–6 × 10^5 copies	6 copies	[67]
			S. pneumoniae	12–1.2 × 10^6 copies	12 copies	
Fluorescence	PDMS	CuO	NSE	0.001–150 ng/mL	0.25 pg/mL	[185]
Fluorescence	PDMS	MNP	*S. Typhimurium*	1.4 × 10^2–1.4 × 10^6 CFU/mL	58 CFU/mL	[186]
Fluorescence	PDMS	ZnO-MSN	*S. Typhimurium*	10^2–10^7 CFU/mL	40 CFU/mL	[187]
Chemiluminescence	Glass	AgNPs	CRP	7 × 10^{-7}-0.07 mg/mL	0.05 ng/mL	[189]
Chemiluminescence	Paper	AuNPs	H-FABP	0.1 pg/mL –1 μg/mL	0.06 pg/mL	[190]
			cTnI	0.5 pg/mL –1 μg/mL	0.3 pg/mL	
			Copeptin	1 pg/mL –1 mg/mL	1.4 pg/mL	

aptasensor for label-free detection of epidermal growth factor receptor (EGFR) (Fig. 8B) [195]. Nanocomposites of amino-functionalized graphene, thionine (THI) and AuNPs were synthesized as the electrochemical probes to modify the WEs. Based on the effect of the aptamer-antigen recognition process on electron transfer, EGFR was determined at a LOD of 5 pg/mL with a linear concentration range of 0.05–200 ng/mL. In comparison with the conventional ELISA method, the analytical reliability of the aptasensor was validated by testing spiked serum samples. Yu and colleagues fabricated an interesting paper-based electrochemical/visual dual-mode analytical device to quantify PSA [196]. The authors exploited Pd@Zn/Co core-shell MOFs nanocomposites with superior electrocatalytic activities to amplify the electrochemical detection signals (i.e. DPV). Meanwhile, the nanocomposites worked as artificial peroxidase to catalyze the chromogenic reaction of TMB to enable the colorimetric detection. Using the dual-mode analytical methods, PSA was determined at a LOD of 0.78 pg/mL with a linear concentration range of 5 pg/mL-50 ng/mL.

With the development of microfabrication techniques, electrochemical biosensors are also widely integrated into polymer-based microfluidic devices. Panat and co-workers reported a glass/PDMS electrochemical microfluidic device to test antibodies to SARS-CoV-2 spike S1 protein and its receptor-binding-domain (RBD) [197]. A nanoprinting method was developed to fabricate Au micropillar electrode arrays on Au films. The microelectrodes were then coated by reduced-GO nanoflakes and immobilized with specific viral antigens. Target antibodies and RBD were quantified at LODs of 2.8 × 10^{-15} and 16.9 × 10^{-15} M, respectively, by an integrated EIS measurement circuit. Bertotti et al. proposed a PDMS microfluidic electrochemical immunosensor for detecting *plasmodium vivax* antibodies (anti-$PvMSP1_{19}$) [198]. Using a dynamic hydrogen bubble template (DHBT) method, nanoporous Au films containing multi-walled carbon nanotubes (MWCNT) were in-situ synthesized on surfaces of Au microelectrodes in channels of the device. The nanocomposites as the immobilization hosts of capture protein fragments displayed excellent electronic conductivity in the electrochemical measurement using cyclic voltammetry. Park and colleagues developed a wearable microfluidic impedimetric immunosensor for POC detection of sweat cortisol [199]. On PDMS substrates, Ti_3C_2Tx MXene nanosheets with good electrical conductivity and high capacity for enzyme immobilization were deposited on WEs that were made of laser-induced graphene flakes. The device exhibited sensitive impedimetric responses to sweat cortisol with a LOD of 88 pM. These electrochemical microfluidic nano-biosensors using different nanomaterials are summarized in Table 2.

4.4. Electrochemiluminescence detections

Electrochemiluminescence (ECL) detection is a combination of electrochemical and chemiluminescence techniques that can provide good selectivity and sensitivity wherein a set of electrodes is used to trigger and control a chemiluminescence reaction [204,205]. ECL method does not need a bulky light source like fluorescence detection and can be generated on an electrode or a chip. Moreover, the background signal is negligible; thus, optical detectors can be used at maximum sensitivity [10,206].

ECL has been widely applied in microfluidic analytical devices

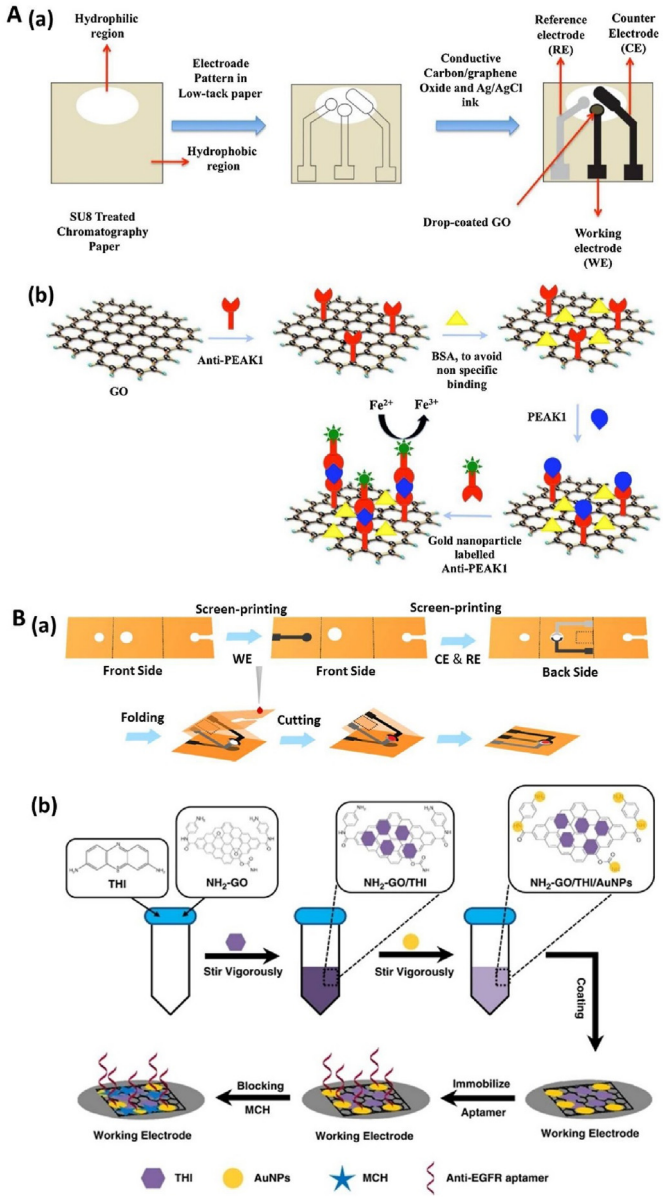

Fig. 8. Scheme of paper-based microfluidic electrochemical nano-biosensors. (A) Design (a) and working principle (b) of paper-based microfluidic electrochemical immunosensor for quantitative detection of PEAK1. Adapted with permission from Ref. [193]. Copyright 2020 Elsevier; (B) Design (a) and working principle (b) of origami-paper-based electrochemical aptasensor for label-free detection of EGFR. Nanocomposites of amino-functionalized graphene, thionine (THI) and AuNPs were synthesized as the electrochemical probes. Adapted with permission from Ref. [195]. Copyright 2020 Springer Nature Publishing.

integrated with nanomaterials such as quantum dots, MOFs, and nanocomposites for bioanalysis. For example, Díez-Buitrago et al. presented a portable and disposable screen-printed electrode-based platform for CdS QDs-based ECL detection [207]. The ECL emission from CdS QDs was triggered with H_2O_2 as a cofactor, and enzymatic assays were employed to modulate the CdS QDs ECL signal by blocking the surface or generating H_2O_2 in situ. Thiol-bearing compounds such as thiocholine generated through the hydrolysis of acetylthiocholine by acetylcholinesterase (AChE) interacted with the surface of CdS QDs, thus blocking the ECL. The biosensor showed a linear range up to 5 mU/mL and a detection limit of 0.73 mU/mL for AChE. Song et al. developed a signal amplified ECL sensor chip for sensitive analysis of procalcitonin (Fig. 9A) [33]. Based on the synergistic catalysis of Au and Pd, the spontaneous cyclic reaction of Ce(III)/Ce(IV), and the high electrochemically active surface area of Ce(III, IV) MOFs, a large number of superoxide anion radicals and hydroxyl radicals were produced (Fig. 9B). Therefore, the luminescence efficiency of N-(aminobutyl)-N-(ethylisoluminol)–dissolved O_2 (ABEI–O_2) systems were improved. Moreover, the affinity peptide ligands were used for the directional connection of antibodies to protect the bioactivity of the proposed sensor. Finally, a PDMS microfluidic platform was used for ECL analysis to integrate the three-electrode detection system into the self-assembled microfluidic chip, which realized the automation and portability of the detection process. The developed sensor showed high sensitivity for procalcitonin detection with a LOD of 3.46 fg/mL, and the detection range of the proposed sensor was 10 fg/mL to 100 ng/mL (Fig. 9C). The RSD and recovery of the sensor for serum sample analysis were 1.4–2.5 and 98.3–102%, respectively. Feng et al. developed a bioactivity-maintained sensing platform for quantitatively detecting neuron-specific enolase (NSE) based on ECL technology and self-assembled portable disease detection chips [208]. First, Fe_3O_4@MoS_2 nanocomposites were prepared as an efficient catalyst to accelerate the reduction of persulfate ($S_2O_8^{2-}$). Specifically, abundant sulfate radicals ($SO_4^{\bullet-}$) were generated because of cyclic conversion between Fe^{2+} and Fe^{3+}. Moreover, a PDMS biosensor chip was constructed by standard lithography processes and integrated with the nano-sensor to detect NSE. A linear equation with a correlation coefficient of 0.998 was obtained. The LOD was 3.67 fg/mL (S/N = 3). A series of spiked serum samples were analyzed to evaluate the proposed microfluidic device. The recovery rate was 98.5–103%, and the RSD was 1.4–3.0%.

4.5. Distance-based detections

In recent years, microfluidic nano-biosensors using the distance-based signal readout show tremendous potential for POC bioanalysis [23,209,210]. Without the need for advanced analytical instruments, the microfluidic biosensing results can be simply displayed as quantitative distance signals in the format of on-chip visual bar charts, making the method particularly advantageous for POT testing. There are mainly two types of driving principles in distance-based microfluidic nano-biosensors: (1) volumetric bar-chart pumping, and (2) capillary effect-based pumping.

In volumetric bar-chart chips (V-Chips), the molecule-recognition events are transduced into the volumes of on-chip produced gas along with pressure variations in sealed microfluidic environments [211]. As a result, inks in defined chambers are pumped into channels, followed by the movement to form visual ink bar charts. It has been evidenced that the ink-bar-chart movement distance is positively related to the volume of produced gas in V-Chips [211]. Hence, by specifically linking the gas production efficiency with assay systems, quantitative bioanalytical signals can be directly displayed as visual ink bar charts without the aid of any sophisticated instruments.

Enzymes and nanomaterials that can produce gas through biological/chemical processes are widely integrated into V-Chips [61,212]. To enhance the operational stability of V-Chips, PtNPs with distinct catalase-like activity and good physicochemical stability have been introduced into V-Chips by Qin's group for immunoassays of cancer biomarkers [212]. Using PtNPs to label the detection antibody, they established ELISA systems in glass/PDMS V-Chips. The V-Chips could be slid to access the reaction and ink chambers to channels after the ELISA procedures. Multiple cancer biomarkers were utilized to validate the bioanalytical performance of the V-Chips. Yang et al. integrated Au/Pt core-shell (Au@Pt) NP-

Table 2
Microfluidic nano-biosensors based on the electrochemical detection method.

Method	Device Substrate	Nanomaterial	Target	Linear Range	LOD	Ref.
Electrochemistry	Paper	Zinc oxide nanowires	p24 antigen	–	0.4 pg/mL	[194]
Electrochemistry	Paper	GO and AuNPs	Pseudopodium-enriched atypical kinase one, SGK269 (PEAK1)	10–10^6 pg/mL	10 pg/mL	[193]
Electrochemistry	Paper	Nanocomposites of amino-functionalized graphene, thionine (THI) and AuNPs	Epidermal growth factor receptor (EGFR)	0.05–200 ng/mL	5 pg/mL	[195]
Electrochemistry	Paper	Pd@Zn/Co core-shell MOFs NPs	PSA	5 pg/mL-50 ng/mL	0.78 pg/mL	[196]
Electrochemistry	Paper	Black phosphorus nanosheets (BP NSs)	Peanut allergen Ara h1	50–1000 ng/mL	21.6 ng/mL	[200]
Electrochemistry	Paper	Single wall carbon nanotubes (SWCNTs)/AuNPs	C-reactive protein; prealbumin	5 pg/mL-1 μg/mL; 10 pg/mL-1μg/mL	5 pg/mL; 10 pg/mL	[201]
Electrochemistry	Glass/ PDMS	Reduced-GO nanoflakes	Antibodies to SARS-CoV-2 spike S1 protein; receptor-binding-domain (RBD)	10^{-12}-20 × 10^{-9} M	2.8 × 10^{-15} M; 16.9 × 10^{-15} M	[197]
Electrochemistry	PDMS	Nanoporous Au films containing multi-walled carbon nanotubes (MWCNT)	Plasmodium vivax antibody (anti-$PvMSP1_{19}$)	2–1000 ng/mL	0.6 ng/mL	[198]
Electrochemistry	PDMS	$Ti_3C_2T_x$ MXene nanosheets	Sweat cortisol	0.01–100 nM	88 pM	[199]
Electrochemistry	PET/PDMS	Multiwall carbon nanotubes/Au nanoflowers	Creatinine	0.01–1 mM	0.5 μM	[202]
Electrochemistry	Glass/ PDMS	AuNPs	PSA	1 pg/mL-10 ng/mL	0.25 pg/mL	[203]

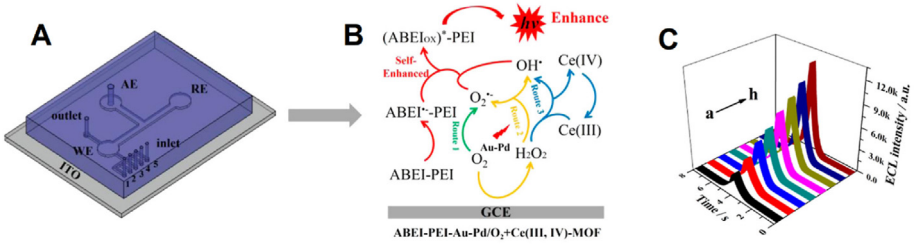

Fig. 9. Microfluidic nano-biosensor for ECL-based detection of procalcitonin. (A) Schematic of the microfluidic chip and (B) the sensing mechanism. (C) ECL intensity–time curves of different procalcitonin concentrations (a–h: 10 fg/mL to 100 ng/mL). Adapted with permission from Ref. [33]. Copyright 2022 American Chemical Society.

encapsulated target-responsive hydrogels in V-Chips for the detection of cocaine [211]. Au@PtNPs were released from the hydrogels due to the specific complexation between target analytes and aptamer linkers and acted as artificial catalase in the V-Chips to form bar-chart signals. Recently, Li and co-workers developed an interesting bar-chart Spinchip with the integration of NP-mediated magnetic aptasensors for multiplexed detection of pathogens (Fig. 10) [210]. It is worthy to note that this work presented a novel approach to address the current challenge in multiplexed bar-chart detection using a "Spinning" mechanism. The introduction of a spin unit not only enables convenient sample introduction from one inlet to multiple different channels, but also elegantly solves the pressure cross-interference problem in the multiplexed volumetric bar-chart chip. In this work, aptamer sequences to target pathogens were labeled with PtNPs and initially captured by capture sequences on the surfaces of magnetic beads that were settled in defied chambers of the chips by using an external magnet. The specific binding between aptamer sequences and target pathogens resulted in the release of PtNPs into the sample solutions to catalyze the decomposition of H_2O_2 into O_2. As a result, simultaneous visual quantitative detection of multiple pathogens was achieved in the bar-chart Spinchip. Three foodborne pathogens (*Salmonella enterica*, *Escherichia coli*, and *Listeria monocytogenes*) were tested at LODs of around 10 CFU/mL in apple juice. Wang et al. presented a glass/PDMS V-Chip with the integration of an aptazyme-induced cascade signal amplification strategy for quantifying aflatoxin B1 (AFB1) and adenosine triphosphate (ATP) [61]. Molecule recognition between target analytes and aptamers formed hemin/G-quadruplex (hGQ) DNAzymes on magnetic silica (MS) NPs as the biosensing probe. By mimicking the horseradish peroxidase (HRP)-accelerated signal enhancement reaction, polymerization of dopamine occurred on MSNPs to generate sufficient anchor sites for covalent capturing of 4-mercaptophenylboric acid (4-MPBA)-modified PtNPs. Wang and colleagues combined the lateral flow immunoassay (LFIA) with V-Chips using PtNPs as the immunoassay probe in LFIA strips [23]. After the immunochromatographic procedure, test zones with captured PtNPs were removed from the strips and loaded into V-Chips to enable visual bar-chart signal readout. The LOD of 0.54 ng/mL PSA was achieved by using this V-Chip.

The capillary effect-based distance detection is mostly applied in μPADs, based on the quantitative flow distance of liquids in paper substrates *via* the capillary effect, which is of particular interest for POC bioanalysis [192,213]. Yang et al. reported a μPAD for POC testing of cocaine using target-responsive aptamer-crosslinked hydrogels [214]. Specific molecule recognition between target analytes and aptamer linkers resulted in the hydrogel collapse with the release of glucoamylase (GA) and the production of glucose. Glucose traveled into paper channels and reacted with deposited glucose oxidase (GOx), HRP and 3,3'-diaminobenzidine (DAB) to display color changes. Employing the length of the colored bars as the quantitative assay signal, cocaine was determined at the LOD of 5.8 μM in urine samples. Liu and colleagues proposed a distance-based μPAD for testing microRNAs (miRNAs) [215]. A rolling circle amplification (RCA) reaction was exploited to enhance the viscosity of target miRNAs in samples. MOFs were utilized to modify the paper substrates to modulate the surface hydrophobicity, through which the distance signal was further amplified. In this way, miR-221 and miR-222 in liver cell lysate were quantified at LODs of 0.33 and 0.37 pM, respectively. Henry et al. presented a microfluidic

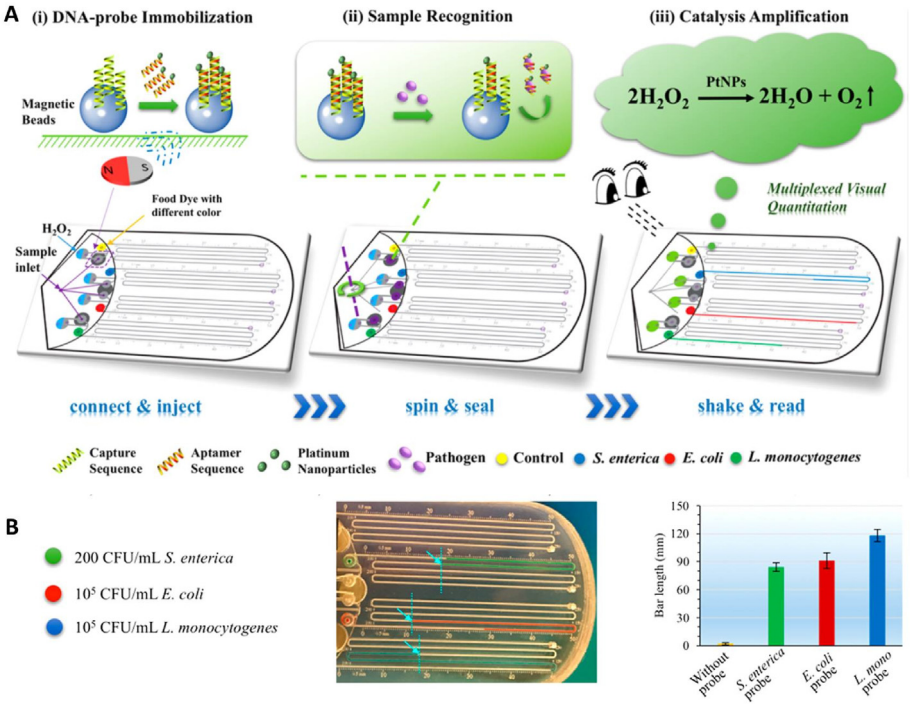

Fig. 10. Scheme of magnetic aptasensor-integrated bar-chart Spinchip for multiplexed detection of pathogens. (A) Working principle of the bar-chart Spinchip; (B) Detection results of three kinds of pathogens. Adapted with permission from Ref. [210]. Copyright 2018 American Chemical Society.

paper sensor for distance-based determination of chloride ions [216]. AgNPs were deposited in paper channels to indicate the visual distance readout *via* the reaction with H_2O_2 and chloride ions to form white AgCl. Chloride ions were detected at a LOD of 2 mg/L in a wide concentration range of 25–1000 mg/L. These distance-based microfluidic nano-biosensors are summarized in Table 3.

4.6. Photothermal detections

As discussed in Section 3.2 in the article, the quantitative detection signals in off-chip photothermal bioassays can be recorded by means of temperature readers (e.g., thermometers) [27,91,220]. The Li group for the first time reported a photothermal biosensing method mediated by nanomaterials for quantitative biochemical analysis using a thermometer [91]. Most of these assays during the early photothermal biosensing development stage were immunoassays [91,220]. Recently, Li and co-workers developed a new low-cost photothermal genetic biosensor on a paper/PMMA hybrid device for quantitative detection of pathogens using a thermometer [27]. DNA capture probes were readily immobilized on the paper surface through a one-step surface modification process. After DNA sandwich hybridization, ssDNA-functionalized AuNPs were introduced into the device to catalyze the oxidation reaction of TMB. The produced oxidized TMB functioned as a strong photothermal agent for the photothermal detection of mycobacterium tuberculosis (MTB) DNA using a miniaturized thermometer

Table 3
Microfluidic nano-biosensors using the distance-based detection method.

Method	Device Substrate	Nanomaterial	Target	Linear Range	LOD	Ref.
Distance-based readout	Glass/PDMS	Au@PtNP-encapsulated target-responsive hydrogels	Cocaine in urine	0–400 μM	0.06 μM	[211]
Distance-based readout	PMMA	PtNPs/magnetic beads	*Salmonella enterica*; *Escherichia coli*; *Listeria monocytogenes*	10–800 CFU/mL; 10^2–10^8 CFU/mL; 10^2–10^7 CFU/mL	10 CFU/mL	[210]
Distance-based readout	Glass/PDMS	Magnetic silica NPs/4-mercaptophenylboric acid-modified PtNPs	Aflatoxin B1 (AFB1); adenosine triphosphate (ATP)	0.005–1 nM; 0.01–1 nM	0.075 pM; 0.818 pM	[61]
Distance-based readout	Glass/PDMS	PtNPs	PSA	0–12 ng/mL	0.54 ng/mL	[23]
Distance-based readout	Paper	Target responsive aptamer-crosslinked hydrogels	Cocaine in urine	10–400 μM	5.8 μM	[217]
Distance-based readout	Paper	MOFs	MicroRNAs (miR-221; miR-222)	0.5–20 pM; 1–20 pM	0.33 pM; 0.37 pM	[215]
Distance-based readout	Paper	AgNPs	Chloride ions	25–1000 mg/L	2 mg/L	[216]
Distance-based readout	Glass/PDMS	PtNPs	Circulating tumor cells (CTCs)	0-200 cells/chamber	1 cell	[218]
Distance-based readout	Glass/PDMS	PtNPs- encapsulated target-responsive hydrogels	Aflatoxin B1 (AFB1)	0–60 nM	1.77 nM	[219]

probe. The LOD of 39 nM MTB DNA was achieved.

Along with the thermometer-based readout method, the photothermal biosensing principle has been integrated into microfluidic chips to develop photothermal bar-chart chips (PT-Chips) using on-chip photothermal signal transduction [23,61,221]. In PT-Chips, the photothermal effect served as a new kind of pumping force, displaying great promise for POC bioanalysis [61]. Upon laser irradiation, the on-chip photothermal effects of nanomaterials can lead to rapid temperature elevations of solutions in defined chambers. The resulting increment of vapor pressure in sealed environments pumps the ink movement in channels to form visual bar-chart signals. Excitingly, the photothermal pumping approach can be operated in a contactless way using portable laser pointers, and the pumping efficiency can be precisely controlled by remotely tuning the irradiation parameters [61]. Therefore, by on-chip integration of the photothermal biosensing and pumping principles, quantitative bioassay signals can also be displayed as visual bar charts in PT-Chips. In comparison with V-Chips, it should be mentioned that PT-Chips are more advantageous in the pumping robustness, operational controllability, and stability to surrounding environments [23,61,221]. Since the working principle of PT-Chips is based on temperature elevation, instead of continuous generation of gas, and is different from conventional V-Chips, we separate it as a different section.

To our best knowledge, Li's group reported the first PT-Chip to demonstrate the feasibility of photothermal microfluidic pumping and the bioanalytical applicability [61]. They fabricated a PMMA/PDMS hybrid bar-chart chip with loaded PB NPs and GO as the photothermal agents. Based on reading the ink-bar-chart movement distance as the analytical signals, it was proved that the photothermal pumping efficiency was quantitatively correlated with the irradiation time and the dose of the photothermal agents, and it can be precisely controlled by tuning these experimental parameters. They successfully exploited the pumping method for on-chip transport of liquid cargos (e.g., AuNPs and dyes) [61]. They further applied the PT-Chip for detector-free immunoassay of PSA as a proof of concept (Fig. 11A) [23]. Immunoassay solutions using PB NPs as the photothermal probe were transferred into the PT-Chips to read the quantitative bar-chart signals in a multiplexed format. Using a traditional spectrophotometric method for comparison, both human serum and whole blood samples were utilized to validate the analytical accuracy of the PT-Chip. PSA was detected at a LOD (i.e. 2.1 ng/mL) below the diagnostic cut-off value of prostate cancer.

Notably, PT-Chips are compatible to a broad range of conventional and commercial bioassays using TMB as the chromogenic substrates, based on exploiting $_{ox}$TMB as the photothermal probes [24,134,221]. For instance, Li and collaborators further integrated a conventional ELISA and the photothermal pumping protocol into a single PT-Chip for multiplexed immunoassay of PSA [221], as diagramed in Fig. 11B. In the ELISA system, on-chip immunocaptured iron oxide NPs acted as artificial peroxidase to catalyze the oxidation of TMB to produce the photothermal probe (i.e., $_{ox}$TMB). Dye solutions in defined chambers were pushed into the channels to form visual quantitative bar-chart immunoassay signals through the photothermal pumping approach. Interestingly, multiplexed detection of six samples was realized in a single chip upon one irradiation process. As a proof of concept, PSA was evaluated at a LOD of 1.9 ng/mL on the chip. The immunoassay performance of the PT-Chip was also validated by a conventional spectrophotometric method.

Additionally, the photothermal biosensing principle can be integrated into μPADs and other platforms in combination with photothermally responsive elements [222]. Fu et al. reported a PMMA/paper hybrid photothermal immunoassay disk with the aid of thermoresponsive hydrogels [223]. Using a clip-magazine chip design, the immuno-recognition took place on the paper substrate using PB NPs as the colorimetric/photothermal dual-functional probe. The photothermal effect resulted in on-chip phase transition of the hydrogels with the release of encapsulated dye solutions in paper channels through the capillary effect. Hence, colorimetric, thermal image- and distance-based tri-mode quantitative output of the immunoassay signals was realized on the disk. Xu and coworkers developed an interesting microfluidic droplet platform using shape memory micropillar arrays to manipulate droplets under the irradiation of NIR light [224]. Au nanorods were mixed into poly(ethylene-vinyl acetate) (EVA) copolymers with shape memory capability to fabricate a photothermally responsive substrate of the micropillar arrays. Under laser irradiation, the photothermal effect-induced micropillar deformation drove the movement of droplets. Based on manipulating the droplet movement, the platform was used to detect ascorbic acid using PB as the colorimetric probe. It should be mentioned that the consumption of reagents in this platform (i.e., sub-microliters) was much lower than that of conventional methods.

5. Conclusions and outlook

In summary, this article reviewed the recent advancement of microfluidic nano-biosensors in POC bioanalysis. Microfluidics has become a powerful LOC technology for POC bioanalysis because of the benefit of integration and miniaturization of analytical settings. Meanwhile, nanomaterials are showing substantial promise in developing biosensors ascribed to their distinctive physical and chemical properties. We believe that the involvement of nanomaterials is playing a key role for the current leap forward in the field. Notably, we have seen improving the reliability of biosensors in terms of sensitivity, selectivity, stability and the potential for POC testing by researchers worldwide. Significantly, it has been a hot research topic to integrate nanomaterial-based biosensors into microfluidic devices. On the one hand, nanomaterials are capable of playing versatile biosensing roles in microfluidic devices, such as molecule recognition, signal transduction and modulation (e.g., amplification and quenching); on the other hand, microfluidics offers a more versatile LOC platform for enabling the biosensing performance of nanomaterials in point of care. Given the exploitation of various biosensing principles including some new instrument-free strategies in recent years, microfluidic nano-biosensors are of particular interest for early diagnostics of diseases, especially in resource-limited areas.

Despite enormous progress in this field, several challenges are still confronted in motivating microfluidic nano-biosensors from bench to practical POC applications. Besides the potential concern in the material aspect (e.g., stability, cost, and toxicity of nanomaterials), some microfluidic biosensors, especially for optical ones, have to rely on bulky analytical instruments for quantitative signal readout or external precise accessories for liquid handling. The operation of some devices like V-Chips is somewhat complicated for unskilled personnel, in addition to the high cost of chip fabrication. For PT-Chips, there is an increasing demand to integrate the chips with the laser systems, possibly to a ready-to-use one. To cope with these limitations, the development of novel instrument-free signal transduction or readout principles is an ideal choice to work with microfluidic devices. Accordingly, new applications or exploration of new physicochemical properties of nanomaterials for biosensing are of great significance. More efforts in multidisciplinary collaboration, especially with artificial intelligence, machine learning and deep learning, are highly desirable to simplify the operation of devices, lower the cost, and achieve automated high-throughput reagent handling and digital readout

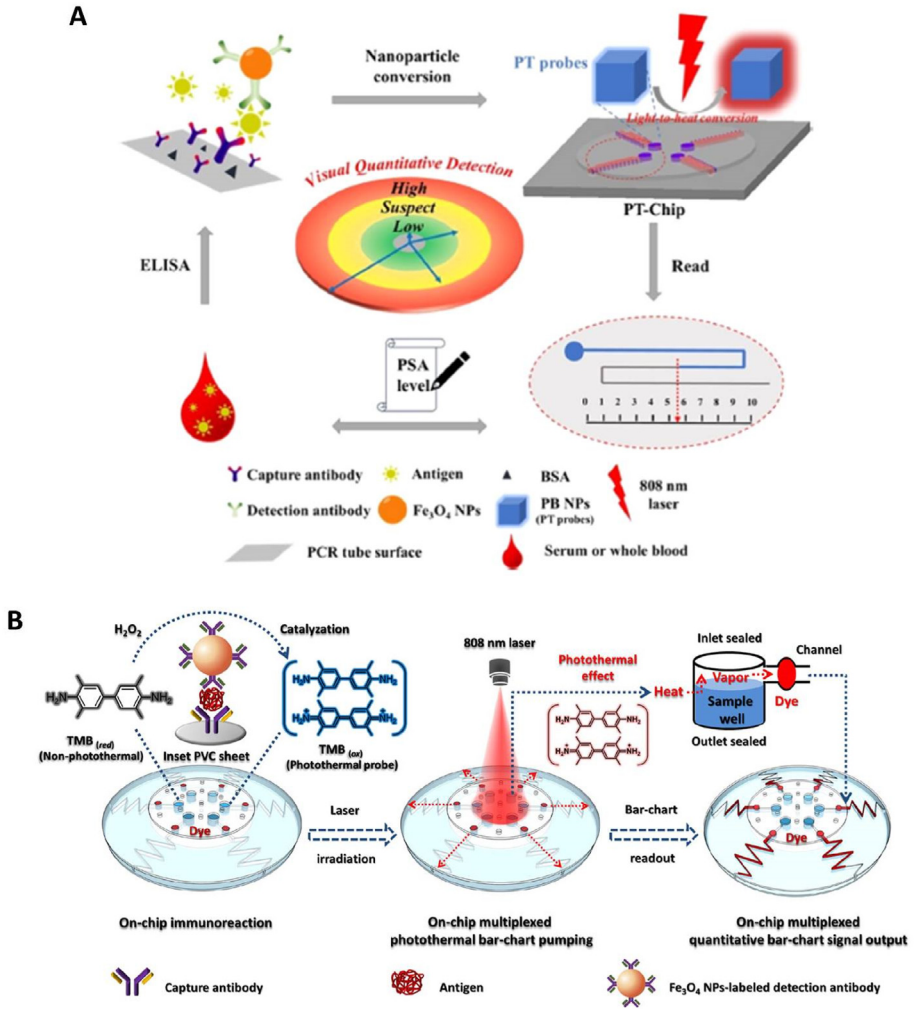

Fig. 11. Working principles of PT-Chips for multiplexed immunoassay of PSA. (A) PT-Chip using PB NPs as the photothermal probe. Adapted with permission from Ref. [23]. Copyright 2021 American Chemical Society. (B) PT-Chip with integration of an ELISA system and the photothermal pumping protocol using $_{ox}$TMB as the photothermal probe. Adapted with permission from Ref. [221]. Copyright 2021 American Chemical Society.

[225,226]. Furthermore, in the material aspect, the matching of compatibility to commercial bioassay kits (e.g., TMB chromogenic systems) might be an alternative way to shorten the gap further because the reliability of these biosensing materials has been commercially validated which can be directly transferred into microfluidic devices. Therefore, considerable research efforts in different aspects are still needed to improve the applicability of microfluidic nano-biosensors in practical POC bioanalysis. With the development of more exciting works by researchers worldwide, microfluidic nano-biosensors are expected to make a new milestone for POC bioanalysis and personalized healthcare in the near future after clinical validation. Therefore, collaboration with healthcare workers and clinical personnel is essential to translate these microfluidic nano-biosensors from bench to practical POC bioanalytical applications.

Declaration of competing interest

The authors declare that they have no known competing financial interests or personal relationships that could have appeared to influence the work reported in this paper.

Data availability

This is a review article. no original data used

Acknowledgments

The authors would like to acknowledge the financial support from the National Institute of Allergy and Infectious Disease of the NIH (R41AI162477), CPRIT (RP210165), the U.S. NSF (IIP2122712, IIP2052347 and CHE2216473), DOT (CARTEEH), the Philadelphia Foundation, and the Medical Center of the Americas Foundation. We are also grateful for the financial support for our prior research from NIH/NIAID (R21AI107415), NIH/NIGMS (SC2GM105584), the NIH RCMI Pilot grant, the NIH BUILDing Scholar Summer Sabbatical Award, NSF (IIP 1953841 and DMR1827745), the University of Texas (UT) System for the STARS Award, and UTEP for IDR, MRAP and URI Programs.

References

[1] Y. Xu, W. Huang, Y. Zhang, H. Duan, F. Xiao, Anal. Chem. 94 (2022) 4463.
[2] F. Haghayegh, R. Salahandish, A. Zare, M. Khalghollah, A. Sanati-Nezhad, Lab Chip 22 (2022) 108.
[3] P.K. Drain, E.P. Hyle, F. Noubary, K.A. Freedberg, D. Wilson, W.R. Bishai,

W. Rodriguez, I.V. Bassett, Lancet Infect. Dis. 14 (2014) 239.
[4] M. Dou, S.T. Sanjay, M. Benhabib, F. Xu, X. Li, Talanta 145 (2015) 43.
[5] L. Bissonnette, M.G. Bergeron, Expert Rev. Mol. Diagn. 17 (2017) 471.
[6] G.J. Kost, Principles & Practice of Point-Of-Care Testing, Lippincott Williams & Wilkins, 2002, p. 672.
[7] L.C. Clark Jr., C. Lyons, Ann. N. Y. Acad. Sci. 102 (1962) 29.
[8] L. Syedmoradi, M. Daneshpour, M. Alvandipour, F.A. Gomez, H. Hajghassem, K. Omidfar, Biosens. Bioelectron. 87 (2017) 373.
[9] M. Dou, J. Lopez, M. Rios, O. Garcia, C. Xiao, M. Eastman, X. Li, Analyst 141 (2016) 3898.
[10] S.T. Sanjay, G. Fu, M. Dou, F. Xu, R. Liu, H. Qi, X. Li, Analyst 140 (2015) 7062.
[11] M. Dou, N. Macias, F. Shen, J. Dien Bard, D.C. Domínguez, X. Li, EClin. Med. 8 (2019) 72.
[12] X.J. Li, C.Y. Yang, P.C.H. Li, Multidisciplinary Microfluidic and Nanofluidic Lab-On-A-Chip: Principles and Applications, 1 ed., Elsevier, 2021.
[13] X.J. Li, Y. Zhou, Microfluidic Devices for Biomedical Applications, 2 ed., Elsevier, 2021.
[14] X.J. Li, Y. Zhou, Microfluidic Devices for Biomedical Applications, 1 ed., Woodhead Publishing (Elsevier), 2013.
[15] J. Zhang, H. Tavakoli, L. Ma, X. Li, L. Han, X. Li, Adv. Drug Deliv. Rev. 187 (2022), 114365.
[16] W. Zhou, H. Tavakoli, L. Ma, C. Bautista, X. Li, Rapid Disease Diagnosis Using Low-Cost Paper and Paper-Hybrid Microfluidic Devices, Elsevier, 2022, p. 325.
[17] M. Lv, W. Zhou, H. Tavakoli, C. Bautista, J. Xia, Z. Wang, X. Li, Biosens. Bioelectron. 176 (2021), 112947.
[18] H. Tavakoli, W. Zhou, L. Ma, Q. Guo, X. Li, Nanotechnology and Microfluidics, Wiley, 2020, p. 177.
[19] M. Dou, J. Sanchez, H. Tavakoli, J.E. Gonzalez, J. Sun, J.D. Bard, X. Li, Anal. Chim. Acta 1065 (2019) 71.
[20] H. Tavakoli, W. Zhou, L. Ma, S. Perez, A. Ibarra, F. Xu, S. Zhan, X. Li, TrAC, Trends Anal. Chem. 117 (2019) 13.
[21] S.T. Sanjay, W. Zhou, M. Dou, H. Tavakoli, L. Ma, F. Xu, X. Li, Adv. Drug Deliv. Rev. 128 (2018) 3.
[22] L. Ma, Y. Abugalyon, X. Li, Anal. Bioanal. Chem. 413 (2021) 4655.
[23] W. Zhou, G. Fu, X. Li, Anal. Chem. 93 (2021) 7754.
[24] W. Zhou, J. Sun, X. Li, Anal. Chem. 92 (2020), 14830.
[25] S.T. Sanjay, M. Li, W. Zhou, X. Li, X. Li, Microsyst. Nanoeng. 6 (2020) 28.
[26] K.S. Prasad, X. Cao, N. Gao, Q. Jin, S.T. Sanjay, G. Henao-Pabon, X. Li, Sensor. Actuator. B Chem. 305 (2020), 127516.
[27] W. Zhou, K. Hu, S. Kwee, L. Tang, Z. Wang, J. Xia, X. Li, Anal. Chem. 92 (2020) 2739.
[28] K.S. Prasad, Y. Abugalyon, C. Li, F. Xu, X. Li, Analyst 145 (2020) 5113.
[29] Y. Gong, Y. Zheng, B. Jin, M. You, J. Wang, X. Li, M. Lin, F. Xu, F. Li, Talanta 201 (2019) 126.
[30] W. Zhou, M. Dou, S.S. Timilsina, F. Xu, X. Li, Lab Chip 21 (2021) 2658.
[31] J. Li, H. Zeng, Z. Zeng, Y. Zeng, T. Xie, ACS Biomater. Sci. Eng. 7 (2021) 5363.
[32] C. Deepa, L. Rajeshkumar, M. Ramesh, J. Mater. Res. Technol. 19 (2022) 2657.
[33] X. Song, S. Yu, L. Zhao, Y. Guo, X. Ren, H. Ma, S. Wang, C. Luo, Y. Li, Q. Wei, Anal. Chem. 94 (2022) 9363.
[34] B.A. Kairdolf, X. Qian, S. Nie, Anal. Chem. 89 (2017) 1015.
[35] Q. Jin, L. Ma, W. Zhou, Y. Shen, O. Fernandez-Delgado, X. Li, Chem. Sci. 11 (2020) 2915.
[36] Q. Jin, B. Lu, Y. Pan, X. Tao, C. Himmelhaver, Y. Shen, S. Gu, Y. Zeng, X. Li, Catal. Today 358 (2020) 324.
[37] C. Hu, W. Yue, M. Yang, Analyst 138 (2013) 6709.
[38] S.K. Katla, J. Zhang, E. Castro, R.A. Bernal, X. Li, ACS Appl. Mater. Interfaces 10 (2018) 75.
[39] K. Hu, L. Ma, Z. Wang, O. Fernandez-Delgado, Y.E. Garay, J.A. Lopez, X. Li, ACS Sustain. Chem. Eng. 10 (2022), 10579.
[40] Q. Jin, L. Ma, W. Zhou, R. Chintalapalle, Y. Shen, X. Li, Catal. Today 358 (2020) 246.
[41] C.M. Jiang, L.Y. Lan, Y. Yao, F.N. Zhao, J.F. Ping, TrAC, Trends Anal. Chem. 102 (2018) 236.
[42] L.Y. Lan, Y. Yao, J.F. Ping, Y.B. Ying, Biosens. Bioelectron. 91 (2017) 504.
[43] H. Aldewachi, T. Chalati, M.N. Woodroofe, N. Bricklebank, B. Sharrack, P. Gardiner, Nanoscale 10 (2018) 18.
[44] L. Reverte, B. Prieto-Simon, M. Campas, Anal. Chim. Acta 908 (2016) 8.
[45] S. Stewart, Q. Wei, Y. Sun, Chem. Sci. 12 (2021) 1227.
[46] W.R. Algar, M. Massey, K. Rees, R. Higgins, K.D. Krause, G.H. Darwish, W.J. Peveler, Z. Xiao, H.-Y. Tsai, R. Gupta, Chem. Rev. 121 (2021) 9243.
[47] Z. Fattahi, M. Hasanzadeh, TrAC, Trends Anal. Chem. 152 (2022), 116637.
[48] M. Lv, W. Zhou, H. Tavakoli, C. Bautista, J. Xia, Z. Wang, X. Li, Biosens. Bioelectron. 176 (2021), 112947.
[49] S. Jain, M. Nehra, R. Kumar, N. Dilbaghi, T. Hu, S. Kumar, A. Kaushik, C.-Z. Li, Biosens. Bioelectron. 179 (2021), 113074.
[50] R. Shandilya, S. Ranjan, S. Khare, A. Bhargava, I.Y. Goryacheva, P.K. Mishra, Drug Discov. Today 26 (2021) 1501.
[51] C. Wang, Y.-Z. Chen, Q.-Z. Yang, C.-H. Tung, D.-Y. Wu, L.-Z. Wu, Mater. Chem. Front. 5 (2021) 458.
[52] G. Biagiotti, A. Angeli, A. Giacomini, G. Toniolo, L. Landini, G. Salerno, L. Di Cesare Mannelli, C. Ghelardini, T. Mello, S. Mussi, ACS Appl. Nano Mater. 4 (2021), 14153.
[53] C. Durmus, S.B. Hanoglu, D. Harmanci, H. Moulahoum, K. Tok, F. Ghorbanizamani, S. Sanli, F. Zihnioglu, S. Evran, C. Cicek, Talanta 243 (2022), 123356.
[54] F. Mousseau, C.F. Tarisse, S. Simon, T. Gacoin, A. Alexandrou, C. Bouzigues, Nanoscale 13 (2021), 14814.
[55] P. Zuo, X. Li, D.C. Dominguez, B.-C. Ye, Lab Chip 13 (2013) 3921.
[56] X. Wei, W. Zhou, S.T. Sanjay, J. Zhang, Q. Jin, F. Xu, D.C. Dominguez, X. Li, Anal. Chem. 90 (2018) 9888.
[57] J. Zhang, X. Wei, R. Zeng, F. Xu, X. Li, Fut. Sci. OA 3 (2017) FSO187.
[58] S.T. Sanjay, M. Dou, J. Sun, X. Li, Sci. Rep. 6 (2016), 30474.
[59] S.T. Sanjay, M. Dou, G. Fu, F. Xu, X. Li, Curr. Pharmaceut. Biotechnol. 17 (2016) 772.
[60] W. Zhou, M. Feng, A. Valadez, X. Li, Anal. Chem. 92 (2020) 7045.
[61] G. Fu, W. Zhou, X. Li, Lab Chip 20 (2020) 2218.
[62] N.M. Neris, R.D. Guevara, A. Gonzalez, F.A. Gomez, Electrophoresis 40 (2019) 296.
[63] R.M. Carvalho, V.S. Ferreira, B.G. Lucca, Anal. Methods 13 (2021) 1349.
[64] H. Persson, S. Park, M. Mohan, K.K. Cheung, C.A. Simmons, E.W. Young, Sensor. Actuator. B Chem. 356 (2022), 131342.
[65] T.N.A. Vo, P.-C. Chen, Sensor Actuator Phys. 334 (2022), 113330.
[66] R.A. Ruiz, J.L. Gonzalez, M. Vazquez-Alvarado, N.W. Martinez, A.W. Martinez, Anal. Chem. 94 (2022) 8833.
[67] M. Dou, S.T. Sanjay, D.C. Dominguez, S. Zhan, X. Li, Chem. Commun. 53 (2017), 10886.
[68] M. Dou, S.T. Sanjay, D.C. Dominguez, P. Liu, F. Xu, X. Li, Biosens. Bioelectron. 87 (2017) 865.
[69] M. Humayun, C.-W. Chow, E.W. Young, Lab Chip 18 (2018) 1298.
[70] S. Wouters, J. De Vos, J.L. Dores-Sousa, B. Wouters, G. Desmet, S. Eeltink, J. Chromatogr. A 1523 (2017) 224.
[71] J. Kim, K. Hong, H. Kim, J. Seo, J. Jeong, P.K. Bae, Y.B. Shin, J.H. Lee, H.J. Oh, S. Chung, Sensor. Actuator. B Chem. 316 (2020), 128094.
[72] Y. Li, T. Xu, X. Chen, S. Lin, M. Cho, D. Sun, M. Yang, Anal. Bioanal. Chem. 409 (2017) 2163.
[73] J. Yin, Z. Zou, Z. Hu, S. Zhang, F. Zhang, B. Wang, S. Lv, Y. Mu, Lab Chip 20 (2020) 979.
[74] X. Hao, P. Yeh, Y. Qin, Y. Jiang, Z. Qiu, S. Li, T. Le, X. Cao, Anal. Chim. Acta 1056 (2019) 96.
[75] S. Agaoglu, M.C. Robles, C.D. Smith, S.R. Quake, I.E. Araci, Microfluid. Nanofluidics 21 (2017) 1.
[76] E. Noviana, D.B. Carrão, R. Pratiwi, C.S. Henry, Anal. Chim. Acta 1116 (2020) 70.
[77] D.M. Cate, J.A. Adkins, J. Mettakoonpitak, C.S. Henry, Anal. Chem. 87 (2015) 19.
[78] N. Ruecha, K. Shin, O. Chailapakul, N. Rodthongkum, Sensor. Actuator. B Chem. 279 (2019) 298.
[79] Y. Fan, S. Shi, J. Ma, Y. Guo, Biosens. Bioelectron. 135 (2019) 1.
[80] M. Sher, R. Zhuang, U. Demirci, W. Asghar, Expert Rev. Mol. Diagn. 17 (2017) 351.
[81] Z. Li, H. Liu, X. He, F. Xu, F. Li, TrAC, Trends Anal. Chem. 108 (2018) 50.
[82] S. Liu, R. Cao, J. Wu, L. Guan, M. Li, J. Liu, J. Tian, Sensor. Actuator. B Chem. 285 (2019) 529.
[83] M. Dou, D.C. Dominguez, X. Li, J. Sanchez, G. Scott, Anal. Chem. 86 (2014) 7978.
[84] M. Yafia, O. Ymbern, A.O. Olanrewaju, A. Parandakh, A. Sohrabi Kashani, J. Renault, Z. Jin, G. Kim, A. Ng, D. Juncker, Nature 605 (2022) 464.
[85] L.A. Kolahalam, I.K. Viswanath, B.S. Diwakar, B. Govindh, V. Reddy, Y. Murthy, Mater. Today Proc. 18 (2019) 2182.
[86] X.Y. Wong, A. Sena-Torralba, R. Alvarez-Diduk, K. Muthoosamy, A. Merkoci, ACS Nano 14 (2020) 2585.
[87] A. Mokhtarzadeh, R. Eivazzadeh-Keihan, P. Pashazadeh, M. Hejazi, N. Gharaatifar, M. Hasanzadeh, B. Baradaran, M. de la Guardia, TrAC, Trends Anal. Chem. 97 (2017) 445.
[88] Q.H. Nguyen, M.I. Kim, TrAC, Trends Anal. Chem. 132 (2020) 12.
[89] M.W. Dou, S.T. Sanjay, M. Benhabib, F. Xu, X.J. Li, Talanta 145 (2015) 43.
[90] M.Z. Yang, Y. Liu, X.Y. Jiang, Chem. Soc. Rev. 48 (2019) 850.
[91] G. Fu, S.T. Sanjay, M. Dou, X. Li, Nanoscale 8 (2016) 5422.
[92] W. Zhou, G. Fu, X. Li, Anal. Chem. 93 (2021) 7754.
[93] D. Liu, F. Liu, Y.S. Huang, Y.L. Song, Z. Zhu, S.F. Zhou, C.Y. Yang, Analyst 144 (2019) 4188.
[94] K.Q. Deng, X.Y. Liu, C.X. Li, H.W. Huang, Biosens. Bioelectron. 117 (2018) 168.
[95] O. Adegoke, S. Zolotovskaya, A. Abdolvand, N.N. Daeid, Talanta 216 (2020) 11.
[96] E.Z. Sheng, Y.X. Lu, Y.T. Tan, Y. Xiao, Z.X. Li, Z.H. Dai, Anal. Chem. 92 (2020) 4364.
[97] L. Shi, W. Liu, B.X. Li, C.J. Yang, Y. Jin, ACS Appl. Mater. Interfaces 13 (2021), 15008.
[98] Y.P. Chen, Y.L. Xianyu, X.Y. Jiang, Accounts Chem. Res. 50 (2017) 310.
[99] X. Zhang, L. Wang, X. Li, X. Li, Chin. Chem. Lett. 33 (2022) 3078.
[100] R. Elghanian, J.J. Storhoff, R.C. Mucic, R.L. Letsinger, C.A. Mirkin, Science 277 (1997) 1078.
[101] X.M. Ma, M. Sun, Y. Lin, Y.J. Liu, F. Luo, L.H. Guo, B. Qiu, Z.Y. Lin, G.N. Chen, Chin. J. Anal. Chem. 46 (2018) 1.
[102] N. Elahi, M. Kamali, M.H. Baghersad, Talanta 184 (2018) 537.
[103] I.H. Cho, D.H. Kim, S. Park, Biomater. Res. 24 (2020) 12.
[104] J. Pingarrón, P. Yá?Ez-Sede?O, A. González-Cortés, Anal. Bioanal. Chem. 53 (2008) 5848.
[105] J.H. Lee, H.Y. Cho, H.K. Choi, J.Y. Lee, J.W. Choi, Int. J. Mol. Sci. 19 (2018) 14.

[106] N.L. Teradal, R. Jelinek, Adv. Healthcare Mater. 6 (2017) 36.
[107] H. Ehtesabi, Mater. Today Chem. 17 (2020) 15.
[108] S. Kruss, A.J. Hilmer, J.Q. Zhang, N.F. Reuel, B. Mu, M.S. Strano, Adv. Drug Deliv. Rev. 65 (2013) 1933.
[109] Q. Wang, B.T. Wang, Sensor. Actuator. B Chem. 275 (2018) 332.
[110] Z. Fattahi, M. Hasanzadeh, TrAC, Trends Anal. Chem. 152 (2022) 20.
[111] S. Kargozar, S.J. Hoseini, P.B. Milan, S. Hooshmand, H.W. Kim, M. Mozafari, Biotechnol. J. 15 (2020) 18.
[112] R. Mohammadi, H. Naderi-Manesh, L. Farzin, Z. Vaezi, N. Ayarri, L. Samandari, M. Shamsipur, J. Pharmaceut. Biomed. Anal. 212 (2022) 16.
[113] F. Ma, C.C. Li, C.Y. Zhang, J. Mater. Chem. B 6 (2018) 6173.
[114] M.C. Dos Santos, W.R. Algar, I.L. Medintz, N. Hildebrandt, TrAC, Trends Anal. Chem. 125 (2020) 18.
[115] H.L. Yang, W.T. Xu, Y. Zhou, Microchim. Acta 186 (2019) 22.
[116] X.X. Zhao, H.B. Zhao, L. Yan, N. Li, J.L. Shi, C.M. Jiang, Crit. Rev. Anal. Chem. 50 (2020) 97.
[117] L. Huang, Z. Yu, J. Chen, D. Tang, ACS Appl. Bio Mater. 3 (2020) 9156.
[118] S. Lee, D. Kwon, C. Yim, S. Jeon, Anal. Chem. 87 (2015) 5004.
[119] Y.Y. Wei, D.N. Wang, Y.Z. Zhang, J.H. Sui, Z.R. Xu, Biosens. Bioelectron. 140 (2019) 48.
[120] S.Y. Du, Y. Wang, Z.C. Liu, Z.X. Xu, H.Y. Zhang, Biosens. Bioelectron. 144 (2019) 8.
[121] T. Bu, Y.M. Tian, J. Ma, M. Zhang, F.E. Bai, S. Zhao, K.Y. He, X.Y. Sun, Y. Wang, L. Wang, Sensor. Actuator. B Chem. 346 (2021) 8.
[122] M.L. You, M. Lin, Y. Gong, S.R. Wang, A. Li, L.Y. Ji, H.X. Zhao, K. Ling, T. Wen, Y. Huang, D.F. Gao, Q. Ma, T.Z. Wang, A.Q. Ma, X.L. Li, F. Xu, ACS Nano 11 (2017) 6261.
[123] J. Wang, Small 1 (2005) 1036.
[124] S. Lee, S. Godhulayyagari, S.T. Nguyen, J.K. Lu, S.B. Ebrahimi, D. Samanta, Angew. Chem. 61 (2022), e202202211.
[125] Y.X. Chen, K.J. Huang, K.X. Niu, Biosens. Bioelectron. 99 (2018) 612.
[126] A.T. Kal-Koshvandi, TrAC, Trends Anal. Chem. 128 (2020) 16.
[127] Y.T. Zhao, X.F. Ruan, Y. Song, J.N. Smith, N. Vasylieva, B.D. Hammock, Y.H. Lin, D. Du, Anal. Chem. 93 (2021), 13658.
[128] Y. Pan, X.L. Wei, X.D. Guo, H. Wang, H.Y. Song, C.P. Pan, N.F. Xu, Biosens. Bioelectron. 194 (2021) 8.
[129] Y.L. Xianyu, Z. Wang, X.Y. Jiang, ACS Nano 8 (2014), 12741.
[130] W.S. Qu, Y.Y. Liu, D.B. Liu, Z. Wang, X.Y. Jiang, Angew. Chem. Int. Ed. 50 (2011) 3442.
[131] Y. Zhou, S.X. Wang, K. Zhang, X.Y. Jiang, Angew. Chem. Int. Ed. 47 (2008) 7454.
[132] Y. Zhang, Q.Y. Liu, C.B. Ma, Q.Q. Wang, M.T. Yang, Y. Du, Theranostics 10 (2020) 5064.
[133] G.N. Cai, Z.Z. Yu, P. Tong, D.P. Tang, Nanoscale 11 (2019), 15659.
[134] G.L. Fu, S.T. Sanjay, W. Zhou, R.A. Brekken, R.A. Kirken, X.J. Li, Anal. Chem. 90 (2018) 5930.
[135] Z. Yu, H. Gong, J. Xu, Y. Li, F. Xue, Y. Zeng, X. Liu, D. Tang, Anal. Chem. 94 (2022) 7408.
[136] S. Lv, K. Zhang, D. Tang, Analyst 144 (2019) 3716.
[137] H.J. Chen, Y. Liu, S.Q. Feng, Y. Cao, T.T. Wu, Z.H. Liu, Biosens. Bioelectron. 200 (2022) 8.
[138] J.P. Lei, H.X. Ju, Chem. Soc. Rev. 41 (2012) 2122.
[139] S. Yao, J. Li, B. Pang, X.C. Wang, Y.J. Shi, X.L. Song, K. Xu, J. Wang, C. Zhao, Microchim. Acta 187 (2020) 8.
[140] T. Sun, N. Xia, F. Yuan, X.M. Liu, Y. Chang, S.D. Liu, L. Liu, Microchim. Acta 187 (2020) 7.
[141] C.N. Loynachan, M.R. Thomas, E.R. Gray, D.A. Richards, J. Kim, B.S. Miller, J.C. Brookes, S. Agarwal, V. Chudasama, R.A. McKendry, M.M. Stevens, ACS Nano 12 (2018) 279.
[142] Z.Q. Gao, H.H. Ye, D.Y. Tang, J. Tao, S. Habibi, A. Minerick, D.P. Tang, X.H. Xia, Nano Lett. 17 (2017) 5572.
[143] I.M. Khoris, K. Takemura, J. Lee, T. Hara, F. Abe, T. Suzuki, E.Y. Park, Biosens. Bioelectron. 126 (2019) 425.
[144] C.P. Kurup, N.F. Mohd-Naim, M.U. Ahmed, Crit. Rev. Biotechnol. 42 (2022) 794.
[145] L. Ding, A.M. Bond, J.P. Zhai, J. Zhang, Anal. Chim. Acta 797 (2013) 1.
[146] H.B. Sun, J.M. Kong, Q.W. Wang, Q.R. Liu, X.J. Zhang, ACS Appl. Mater. Interfaces 11 (2019), 27568.
[147] C. Toyos-Rodriguez, A. Adawy, F.J. Garcia-Alonso, A. de la Escosura-Muniz, Biosens. Bioelectron. 200 (2022) 10.
[148] J. Li, J. He, C. Zhang, J. Chen, W. Mao, C. Yu, Biosens. Bioelectron. 130 (2019) 166.
[149] L. Liu, L. Tian, G. Zhao, Y. Huang, W. Cao, Anal. Chim. Acta 986 (2017) 138.
[150] L. Bezinge, A. Suea-Ngam, A.J. deMello, C.J. Shih, Molecular Systems Design & Engineering 5 (2020) 49.
[151] X.D. Cao, Y.K. Ye, S.Q. Liu, Anal. Biochem. 417 (2011) 1.
[152] M.Y. Li, W.J. Zhang, Y.Z. Zhang, Anal. Methods 13 (2021) 4150.
[153] C.L. Tang, Z.Y. He, H.M. Liu, Y.Y. Xu, H. Huang, G.J. Yang, Z.Q. Xiao, S. Li, H.N. Liu, Y. Deng, Z. Chen, H. Chen, N.Y. He, J. Nanobiotechnol. 18 (2020) 19.
[154] D. Cheng, M.Q. Yu, F. Fu, W.Y. Han, G. Li, J.P. Xie, Y. Song, M.T. Swihart, E.Q. Song, Anal. Chem. 88 (2016) 820.
[155] C. Zhou, H.M. Zou, C.J. Sun, Y.X. Li, Food Chem. 361 (2021) 17.
[156] A. Huang, W.W. Li, S. Shi, T.M. Yao, Sci. Rep. 7 (2017) 7.
[157] A. Afzalinia, M. Mirzaee, ACS Appl. Mater. Interfaces 12 (2020), 16076.
[158] J.J. Li, J. Wu, Z.Q. He, H. Pei, Q.F. Xia, Q. Wu, H.X. Ju, Sensor. Actuator. B Chem. 290 (2019) 41.
[159] K.W. Lee, K.R. Kim, H.J. Chun, K.Y. Jeong, D.K. Hong, K.N. Lee, H.C. Yoon, Biosens. Bioelectron. 163 (2020) 8.
[160] Y.T. Shang, X.R. Xiang, Q.H. Ye, Q.P. Wu, J.M. Zhang, J.M. Lin, TrAC, Trends Anal. Chem. 147 (2022) 20.
[161] G. Fu, S.T. Sanjay, X. Li, Analyst 141 (2016) 3883.
[162] S.K. Kailasa, J.R. Koduru, M.L. Desai, T.J. Park, R.K. Singhal, H. Basu, TrAC, Trends Anal. Chem. 105 (2018) 106.
[163] M. Chen, Y. Wang, X. Zhao, J. Zhang, Y. Peng, J. Bai, S. Li, D. Han, S. Ren, K. Qin, Talanta 243 (2022), 123338.
[164] Y. Man, M. Ban, A. Li, X. Jin, Y. Du, L. Pan, Food Chem. 354 (2021), 129578.
[165] W. Qi, L. Zheng, S. Wang, F. Huang, Y. Liu, H. Jiang, J. Lin, Biosens. Bioelectron. 178 (2021), 113020.
[166] Z. Hu, J. Jian, Y. Hua, D. Yang, Y. Gao, J. You, Z. Wang, Y. Chang, K. Yuan, Z. Bao, Sensor. Actuator. B Chem. 273 (2018) 559.
[167] X. Luan, Y. Pan, D. Zhou, B. He, X. Liu, Y. Gao, J. Yang, Y. Song, Biosens. Bioelectron. 165 (2020), 112406.
[168] T. Pinheiro, A.C. Marques, P. Carvalho, R. Martins, E. Fortunato, ACS Appl. Mater. Interfaces 13 (2021) 3576.
[169] N. Alizadeh, A. Salimi, R. Hallaj, Sensor. Actuator. B Chem. 288 (2019) 44.
[170] M.-M. Liu, S.-H. Li, D.-D. Huang, Z.-W. Xu, Y.-W. Wu, Y. Lei, A.-L. Liu, Sensor. Actuator. B Chem. 305 (2020), 127512.
[171] X. Xu, X. Wang, J. Hu, Y. Gong, L. Wang, W. Zhou, X. Li, F. Xu, Electrophoresis 40 (2019) 914.
[172] Z. Wang, X. Wu, L. Xu, H. Kuang, C. Xu, Anal. Methods 11 (2019) 5478.
[173] S. Dalirirad, A.J. Steckl, Sensor. Actuator. B Chem. 283 (2019) 79.
[174] C. Akkapinyo, P. Khownarumit, D. Waraho-Zhmayev, R.P. Poo-Arporn, Anal. Chim. Acta 1095 (2020) 162.
[175] S.T. Sanjay, M. Dou, J. Sun, X. Li, Sci. Rep. 6 (2016) 1.
[176] N. Alizadeh, F. Ghasemi, A. Salimi, R. Hallaj, F. Fathi, F. Soleimani, Dyes Pigments 173 (2020), 107875.
[177] P. Zhang, X. Wu, H. Xue, Y. Wang, X. Luo, L. Wang, Anal. Chim. Acta 1212 (2022), 339911.
[178] V. Shirshahi, S.N. Tabatabaei, S. Hatamie, R. Saber, Colloids Surf. B Biointerfaces 186 (2020), 110721.
[179] H. Tong, C. Cao, M. You, S. Han, Z. Liu, Y. Xiao, W. He, C. Liu, P. Peng, Z. Xue, Biosens. Bioelectron. (2022), 114449.
[180] C. Celik, G. Can Sezgin, U.G. Kocabas, S. Gursoy, N. Ildiz, W. Tan, I. Ocsoy, Anal. Chem. 93 (2021) 6246.
[181] E.L. Rossini, M.I. Milani, L.S. Lima, H.R. Pezza, Spectrochim. Acta Mol. Biomol. Spectrosc. 248 (2021), 119285.
[182] M. Dou, J.M. García, S. Zhan, X. Li, Chem. Commun. 52 (2016) 3470.
[183] N. Yildirim, F. Long, C. Gao, M. He, H.-C. Shi, A.Z. Gu, Environ. Sci. Technol. 46 (2012) 3288.
[184] Z. Lin, L. Chen, G. Zhang, Q. Liu, B. Qiu, Z. Cai, G. Chen, Analyst 137 (2012) 819.
[185] T. Wu, S. Yu, L. Dai, J. Feng, X. Ren, H. Ma, X. Wang, Q. Wei, H. Ju, ACS Sens. 7 (2022) 1732.
[186] S. Wang, L. Zheng, G. Cai, N. Liu, M. Liao, Y. Li, X. Zhang, J. Lin, Biosens. Bioelectron. 140 (2019), 111333.
[187] F. Huang, R. Guo, L. Xue, G. Cai, S. Wang, Y. Li, M. Liao, M. Wang, J. Lin, Sensor. Actuator. B Chem. 312 (2020), 127958.
[188] M. Dou, N. Macias, F. Shen, J.D. Bard, D.C. Domínguez, X. Li, EClin. Med. 8 (2019) 72.
[189] C. Zong, D. Zhang, F. Jiang, H. Yang, S. Liu, P. Li, Talanta 199 (2019) 164.
[190] F. Li, L. Guo, Y. Hu, Z. Li, J. Liu, J. He, H. Cui, Talanta 207 (2020), 120346.
[191] J. Adkins, K. Boehle, C. Henry, Electrophoresis 36 (2015) 1811.
[192] E. Noviana, T. Ozer, C.S. Carrell, J.S. Link, C. McMahon, I. Jang, C.S. Henry, Chem. Rev. 121 (2021), 11835.
[193] K.S. Prasad, X.Y. Cao, N. Gao, Q.J. Jin, S.T. Sanjay, G. Henao-Pabon, X.J. Li, Sensor. Actuator. B Chem. 305 (2020) 8.
[194] X. Li, Z. Qin, H. Fu, T. Li, R. Peng, Z.J. Li, J.M. Rini, X.Y. Liu, Biosens. Bioelectron. 177 (2021) 8.
[195] Y. Wang, S. Sun, J.P. Luo, Y. Xiong, T. Ming, J.T. Liu, Y.Y. Ma, S. Yan, Y. Yang, Z.G. Yang, J. Reboud, H.B. Yin, J.M. Cooper, X.X. Cai, Microsyst. Nanoeng. 6 (2020) 9.
[196] C. Zhou, K. Cui, Y. Liu, S. Hao, L. Zhang, S. Ge, J. Yu, Anal. Chem. 93 (2021) 5459.
[197] M.A. Ali, C.S. Hu, S. Jahan, B. Yuan, M.S. Saleh, E.G. Ju, S.J. Gao, R. Panat, Adv. Mater. 33 (2021) 15.
[198] M. Regiart, A.M. Gimenez, R.F. Marques, I.S. Soares, M. Bertotti, Sensor. Actuator. B Chem. 340 (2021) 8.
[199] J.S. Nah, S.C. Barman, M. Abu Zahed, M. Sharifuzzaman, H. Yoon, C. Park, S. Yoon, S.P. Zhang, J.Y. Park, Sensor. Actuator. B Chem. 329 (2021) 9.
[200] H. Jiang, Q. Guo, C. Zhang, Z.K. Sun, X. Weng, Food Chem. 365 (2021) 8.
[201] S. Sun, J.P. Luo, Y.X. Zhu, F.L. Kong, G. Mao, T. Ming, Y. Xing, J.T. Liu, Y.C. Dai, S. Yan, Y. Yang, X.X. Cai, Biosens. Bioelectron. 208 (2022) 9.
[202] J.Y. Li, Z.H. Li, Y.Z. Dou, J. Su, J.Y. Shi, Y. Zhou, L.H. Wang, S.P. Song, C.H. Fan, Chem. Commun. 57 (2021) 4726.
[203] X.L. Wang, X.Y. He, Z.H. He, L.W. Hou, C. Ge, L. Wang, S.B. Li, Y. Xu, Biosens. Bioelectron. 204 (2022) 9.
[204] C. Fang, H. Li, J. Yan, H. Guo, T. Yifeng, Chemelectrochem 4 (2017) 1587.
[205] L. Hu, G. Xu, Chem. Soc. Rev. 39 (2010) 3275.
[206] M. Chen, Z. Ning, K. Chen, Y. Zhang, Y. Shen, J. Anal. Test. 4 (2020) 57.
[207] B. Díez-Buitrago, L. Saa, N. Briz, V. Pavlov, Talanta 225 (2021), 122029.
[208] T. Feng, X. Song, Y. Du, Y. Bai, X. Ren, H. Ma, D. Wu, Y. Li, Q. Wei, Anal. Chem.

94 (2022) 9176.
[209] Y. Song, Y. Li, L. Qin, Methods Mol. Biol. 1570 (2017) 105.
[210] X.F. Wei, W. Zhou, S.T. Sanjay, J. Zhang, Q.J. Jin, F. Xu, D.C. Dominguez, X.J. Li, Anal. Chem. 90 (2018) 9888.
[211] Z. Zhu, Z.C. Guan, S.S. Jia, Z.C. Lei, S.C. Lin, H.M. Zhang, Y.L. Ma, Z.Q. Tian, C.J. Yang, Angew. Chem. Int. Ed. 53 (2014), 12503.
[212] Y.J. Song, X.F. Xia, X.F. Wu, P. Wang, L.D. Qin, Angew. Chem. Int. Ed. 53 (2014), 12451.
[213] S. Chung, C.M. Jennings, J.Y. Yoon, Chem.–Eur. J. 25 (2019), 13070.
[214] X. Wei, T. Tian, S. Jia, Z. Zhu, Y. Ma, J. Sun, Z. Lin, C.J. Yang, Anal. Chem. 88 (2016) 2345.
[215] L. Zhang, J. Chen, H.H. Yang, Z.N. Yu, Y.Z. Xu, S.Y. Liu, Z. Dai, X.Y. Zou, Sensor. Actuator. B Chem. 359 (2022) 8.
[216] K. Phoonsawat, N. Ratnarathorn, C.S. Henry, W. Dungchai, Analyst 143 (2018) 3867.
[217] X. Wei, T. Tian, S. Jia, Z. Zhi, C.J. Yang, Anal. Chem. 88 (2016) 2345.
[218] M.F. Abate, S.S. Jia, M.G. Ahmed, X.R. Li, L. Lin, X.Q. Chen, Z. Zhu, C.Y. Yang, Small 15 (2019) 8.
[219] Y.L. Ma, Y. Mao, D. Huang, Z. He, J.M. Yan, T. Tian, Y.Z. Shi, Y.L. Song, X.R. Li, Z. Zhu, L.J. Zhou, C.J. Yang, Lab Chip 16 (2016) 3097.
[220] G. Fu, S.T. Sanjay, W. Zhou, R.A. Brekken, R.A. Kirken, X. Li, Anal. Chem. 90 (2018) 5930.
[221] G.L. Fu, R.X. Hou, X.B. Mou, X.J. Li, Anal. Chem. 93 (2021), 15105.
[222] G.L. Fu, Y.B. Zhu, K. Xu, W.H. Wang, R.X. Hou, X.J. Li, Anal. Chem. 91 (2019), 13290.
[223] G.L. Fu, X.J. Li, W.H. Wang, R.X. Hou, Biosens. Bioelectron. 170 (2020) 9.
[224] W.-Q. Ye, Y.-Y. Wei, D.-N. Wang, C.-G. Yang, Z.-R. Xu, Lab Chip 21 (2021) 1131.
[225] Z. Angehrn, L. Haldna, A.S. Zandvliet, E.G. Berglund, J. Zeeuw, B. Amzal, S.Y.A. Cheung, T.M. Polasek, M. Pfister, T. Kerbusch, N.M. Heckman, Front. Pharmacol. 11 (2020) 12.
[226] C.Y. Cao, M.L. You, H.Y. Tong, Z.R. Xue, C. Liu, W.H. He, P. Peng, C.Y. Yao, A. Li, X.Y. Xu, F. Xu, Lab Chip 22 (2022) 3837.